Solenoid-free plasma start-up in spherical tokamaks

2014 Plasma Phys. Control. Fusion 56 103001

(http://iopscience.iop.org/0741-3335/56/10/103001)

IOP Publishing Plasma Physics and Controlled Fusion

Plasma Phys. Control. Fusion **56** (2014) 103001 (19pp) doi:10.1088/0741-3335/56/10/103001

Topical Review

Solenoid-free plasma start-up in spherical tokamaks

R Raman[1] **and V F Shevchenko**[2]

[1] William E. Boeing Department of Aeronautics and Astronautics, University of Washington, Seattle, WA 98195, USA
[2] CCFE, Culham Science Centre, Abingdon, Oxon, OX14 3DB, UK

E-mail: raman@aa.washington.edu

Received 15 June 2014, revised 20 August 2014
Accepted for publication 1 September 2014
Published 22 September 2014

Abstract

The central solenoid is an intrinsic part of all present-day tokamaks and most spherical tokamaks. The spherical torus (ST) confinement concept is projected to operate at high toroidal beta and at a high fraction of the non-inductive bootstrap current as required for an efficient reactor system. The use of a conventional solenoid in a ST-based fusion nuclear facility is generally believed to not be a possibility. Solenoid-free plasma start-up is therefore an area of extensive worldwide research activity. Solenoid-free plasma start-up is also relevant to steady-state tokamak operation, as the central transformer coil of a conventional aspect ratio tokamak reactor would be located in a high radiation environment but would be needed only during the initial discharge initiation and current ramp-up phases. Solenoid-free operation also provides greater flexibility in the selection of the aspect ratio and simplifies the reactor design. Plasma start-up methods based on induction from external poloidal field coils, helicity injection and radio frequency current drive have all made substantial progress towards meeting this important need for the ST. Some of these systems will now undergo the final stages of test in a new generation of large STs, which are scheduled to begin operations during the next two years. This paper reviews research to date on methods for inducing the initial start-up current in STs without reliance on the conventional central solenoid.

Keywords: solenoid-free, start-up, spherical tokamak

(Some figures may appear in colour only in the online journal)

1. Introduction

Since the inception of the tokamak concept [1], plasma current start-up has relied on a central solenoid (CS), which through transformer action generates initial breakdown and initiates the plasma current. CS is an integral part of all present-day tokamaks. It is a well-developed and well-understood system for current start-up. A low aspect ratio version of the tokamak is referred to as a spherical torus or a spherical tokamak (ST) [2]. ST was proposed as an alternate method to a conventional tokamak for generating fusion plasmas. Soon it became apparent that reactors based on the ST concept couldn't be built with a full sized CS because of the very restricted space at the center of the torus. Even the use of a partial or retractable [3] solenoid requires a compromise on the achievable aspect ratio A, defined as the ratio of the major to minor radius ($A = R/a$). Furthermore, since CS cannot drive current during steady-state operation, tokamaks and STs will require some other form of non-inductive current drive (CD) to sustain the plasma discharge. These CD systems can be used to ramp the plasma current up to the sustainment level, if an alternative method were employed to generate the initial plasma and plasma current up to the level sufficient for the non-inductive CD ramp-up to be applied. This is indeed the current approach used for the development of the ST program [4] to assess the STs potential for a next-step Fusion Nuclear Science Facility (FNSF) [5].

Building a tokamak/ST-based reactor that does not rely on the CS would simplify the design, and reduce cost, because a relatively large and complex system, the CS, need not be

Table 1. Recent devices contributing to the development of methods for plasma current start-up without reliance on the CS. Devices shown in bold are currently in operation. PLT, JT-60U and DIII-D are tokamaks. MAST-U and NSTX-U are undergoing major machine upgrades. As noted, present research emphasis on some of the STs is primarily on ST physics and less on plasma start-up.

Device	Country	Institution	B_T (T)	R/a (m)	Method being developed
START	UK	Culham	0.3	0.3/0.24	Merging compression/DNM
CDX-U	USA	PPPL	0.23	0.34/0.22	LHI, ECH start-up
HIT-II	USA	Univ. Washington	0.5	0.3/0.2	Transient CHI SS CHI
MAST	UK	Culham	0.63	0.85/0.65	EBW start-up Merging compression/DNM
NSTX	USA	PPPL	0.55	0.86/0.68	Transient CHI PF induction
HIST	Japan	Univ. Hyogo	0.2	0.3/0.24	SS CHI
PEGASUS	USA	Univ. Wisconsin	0.18	0.45/0.35	LHI
TST-2	Japan	Univ. Tokyo	0.4	0.38/0.25	LHCD
TS3	Japan	Univ. Tokyo	0.15	0.2/0.14	Merging reconnection
TS4			0.1	0.5/0.4	
UTST	Japan	Univ. Tokyo	0.15	0.43/0.17	Double null merging (DNM)
LATE	Japan	Univ. Kyoto	0.12	0.25/0.28	ECH, EBW
QUEST	Japan	Kyushu Univ.	0.25–0.5	0.68/0.4	ECH, EBW
LTX	USA	PPPL	0.32	0.4/0.26	ST Physics
SUNIST	China	Tsinghua Univ.	0.15	0.3/0.23	ST Physics
ETE	Brazil	NSRI	0.4	0.3/0.2	ST Physics
Globus-M	Russia	IOFFE	0.62	0.36/0.24	ST Physics
VEST	Korea	Seoul Univ.	0.1	0.4/0.3	Merging compression
MAST-U	UK	Culham	0.84	0.85/0.65	EBW start-up Merging compression/DNM
NSTX-U	USA	PPPL	1.0	0.93/0.65	Transient CHI, LHI, EBW start-up
Tokamak					
CDX	USA	PPPL	0.45	0.59/0.05	LHI
CCT	USA	UCLA	0.2	1.5/0.4	LHI
PLT	USA	PPPL	4.0	1.32/0.4	LHCD
JT-60U	Japan	JAEA	4.2	3.4/1.0	PF induction
DIII-D	USA	General Atomics	2.2	1.67/0.67	PF induction, ECH start-up

integrated into the system design. In steady-state tokamak and ST reactors, the CS is needed only for generating the initial plasma current, as it cannot be used to maintain the current in steady state discharges indefinitely. However, it needs to be shielded from neutrons and maintained, largely for the purpose of initiating the plasma current. In addition, because the toroidal field is considerably high on the inboard region of a low aspect ratio device, the freed up space now allows the higher field on the inboard side to be used more efficiently by optimizing the device aspect ratio. More than a decade ago, these factors, motivated extensive worldwide interest and activity in developing methods for solenoid-free plasma start-up in STs. Since the first experiments on the START [6] tokamak in UK, a number of new approaches have made considerable progress to establish solenoid-less current start-up. Some of these techniques are now undergoing final assessment in large STs to explore their capability for replacing the conventional solenoid. The significant developments in each of these areas will be described in this topical review paper on solenoid-free plasma start-up in STs.

1.1. Methods for solenoid-free plasma start-up

The methods for plasma start-up fall into three broad classes. Coaxial helicity injection (CHI) and local helicity injection (LHI) are based on the injection of magnetic helicity. Outer poloidal field (PF) induction and merging compression rely on the use of induction, but without the use of CS. Electron cyclotron heating (ECH), lower hybrid current drive (LHCD) and electron Bernstein wave (EBW) systems are based on current start-up using radio frequency (RF) waves. The approaches developed for solenoid-free plasma start-up vary widely both in their ingenuity and implementation. Table 1 summarizes the devices and the methods deployed there to enable solenoid-free plasma start-up.

Transient CHI developed on the HIT-II device [7] at the University of Washington was successfully used on the NSTX device at PPPL [8] to improve the performance of inductive-only plasmas. Point source helicity injection also referred to as local helicity injection has been used on the Pegasus device [9] at the University of Wisconsin, to generate plasma currents, which have been successfully coupled to inductive drive.

The first method to generate substantial amounts of plasma current, that was compatible with conventional inductive drive was the merging-compression method developed on the START tokamak [6] at the Culham [10] Science Centre, UK. It was then successfully applied on MAST [10, 11], a larger successor ST in the same laboratory. The TS3/4 device [12] at the University of Tokyo is exploring merging-reconnection start-up, and methods based on using induction from the outer PF coils in the UTST device [13]. Other non-ST based devices that are contributing to the solenoid-free plasma start-up research include the DIII-D tokamak that has used induction from the outer PF coils for generating 100 kA of plasma

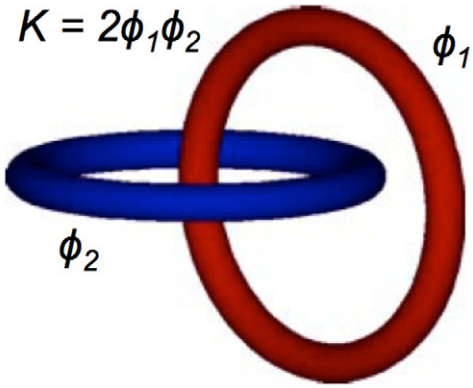

Figure 1. Shown are two magnetic flux tubes linked to each other. The total helicity (K) can be shown to be twice the product of the magnetic flux contained in each flux tube [25].

current [14]. The same method has also been used on the JT-60U tokamak in Japan to generate a similar level of plasma current [15].

The very earliest test of ECH plasma current start-up in an ST was conducted on CDX-U [16] at PPPL. The work was later extended to the much larger DIII-D [17] tokamak. In both these devices ECH power provided the necessary conditions for breakdown, heating and current generation. ECH is being developed on the QUEST [18] ST at Kyushu University and on the LATE device [19] at Kyoto University, both in Japan. The University of Tokyo is developing methods based on LHCD on the TST-2 [20] device. 100 kA of plasma current was also generated using LHCD start-up on the PLT tokamak at PPPL [21].

EBW plasma start-up has been used on MAST [22] to generate substantial plasma currents.

A recent review article is primarily devoted to the physics of inductive plasma start-up using CS [23]. It also briefly touches the methods of non-inductive plasma start-up. This review complements that paper by describing in greater detail the status of research and physics of solenoid-less plasma start-up. Sections 2, 3 and 4 will discuss the physics of plasma current generation using helicity injection; start-up using outer PF induction, and start-up using waves, respectively.

In addition to these methods, the use of an iron core transformer has also been proposed. The design overcomes the issues of insulating a multi-turn solenoid located in the center post by relocating the flux inducing solenoid to the outer legs of the transformer. The transformer core located inside the center stack is surrounded by the toroidal field conductors, which are shaped in the form of individual wedges, each separated from the adjacent ones by resistive inserts to reduce eddy currents in the toroidal field conductor when the transformer is energized [24]. There is also a proposal on retractable solenoid [3], which is supposed to produce initial plasma and then is removed from the machine during steady-state operation.

2. Plasma start-up by helicity injection

Helicity is the linkage of magnetic flux with magnetic flux (figure 1). In the context of plasma start-up in STs it is the linkage of poloidal magnetic flux with toroidal magnetic flux. In toroidal geometry it is given by $K = 2\int \phi \, \mathrm{d}\psi$ where ϕ is the toroidal flux inside a flux surface and ψ is the poloidal flux.

Bellan [25] discusses the concept of helicity and λ in great detail. Here we briefly summarize the most important aspects needed for this paper. In an isolated system with a conducting boundary so that the normal component of the magnetic field is zero, Taylor's hypothesis states that magnetic reconnection conserves global helicity while minimizing the magnetic energy [26]. This is because magnetic field energy decays faster than the helicity, so the configuration tends to relax towards a state of minimum energy while conserving helicity. Helicity is conserved on reconnection time scales and decays on the resistive time scale, whereas magnetic energy decays on the reconnection time scale. Woltjer [27] showed that the resulting magnetic field satisfies the simple force-free equation

$$\nabla \times B = \lambda B \tag{1}$$

Using Amperes law, equation (1) can be written as $\mu_0 J = \lambda B$, and it can be seen that, λ has the unit of inverse length. From equation (1), λB is analogous to the vorticity of a velocity field in fluid mechanics. The vorticity of a flow is equal to the curl of the velocity field ($\omega = \nabla \times v$) and describes the local spinning motion of a fluid near some point as would be seen by an observer located at that point traveling with the fluid. λB is the amount of twist or curl of the vector B at each point.

Helicity injection requires the presence of two electrodes linked by magnetic flux. This is the injector flux. A voltage is then applied to these electrodes to drive current along the magnetic field lines. The helicity injection rate can be shown to be equal to $2V_{\mathrm{inj}}\psi_{\mathrm{inj}}$, where V_{inj} is the voltage between electrodes and ψ_{inj} is the magnetic flux that penetrates both electrodes. For successful helicity injection, four requirements should be met [28]. (1) The injected helicity must relax towards a configuration that has the desired magnetic equilibrium; (2) the region into which the helicity is being injected must provide a helicity barrier so that the injected helicity is confined; (3) sufficient helicity must be injected so that it overcomes any losses and a stable configuration can be formed, and in the case of steady-state CD, the system must be sustained against losses by steady-state helicity injection; (4) the energy per unit helicity of the injected helicity must be higher than that dissipated by the equilibrium. This last condition is described by the relation, $\lambda_{\mathrm{inj}} > \lambda_{\mathrm{tokamak}}$, where $\lambda_{\mathrm{inj}} = \mu_0 I_{\mathrm{inj}}/\psi_{\mathrm{inj}}$ and $\lambda_{\mathrm{tokamak}} = \mu_0 I_{\mathrm{p}}/\phi_{\mathrm{tokamak}}$. Here, I_{inj} is the current in the injector region or the helicity source chamber, I_{p} is the plasma current in the tokamak and ϕ_{tokamak} is the toroidal flux enclosed by the magnetic equilibrium.

Helicity injection CD in a tokamak was first developed on the ACT-1/CDX device at PPPL [29], where biasing an electrode with respect to an anode generated a toroidal current. Since those initial experiments, two different systems have been developed to demonstrate high quality plasma current start-up using this concept. These are transient CHI [7], first demonstrated on the HIT-II device, which employs large surface area electrodes, and point source (or localized) helicity injection, demonstrated on the Pegasus device [9], which relies on smaller surface area active current sources to inject helicity, similar in concept to the early work on CDX.

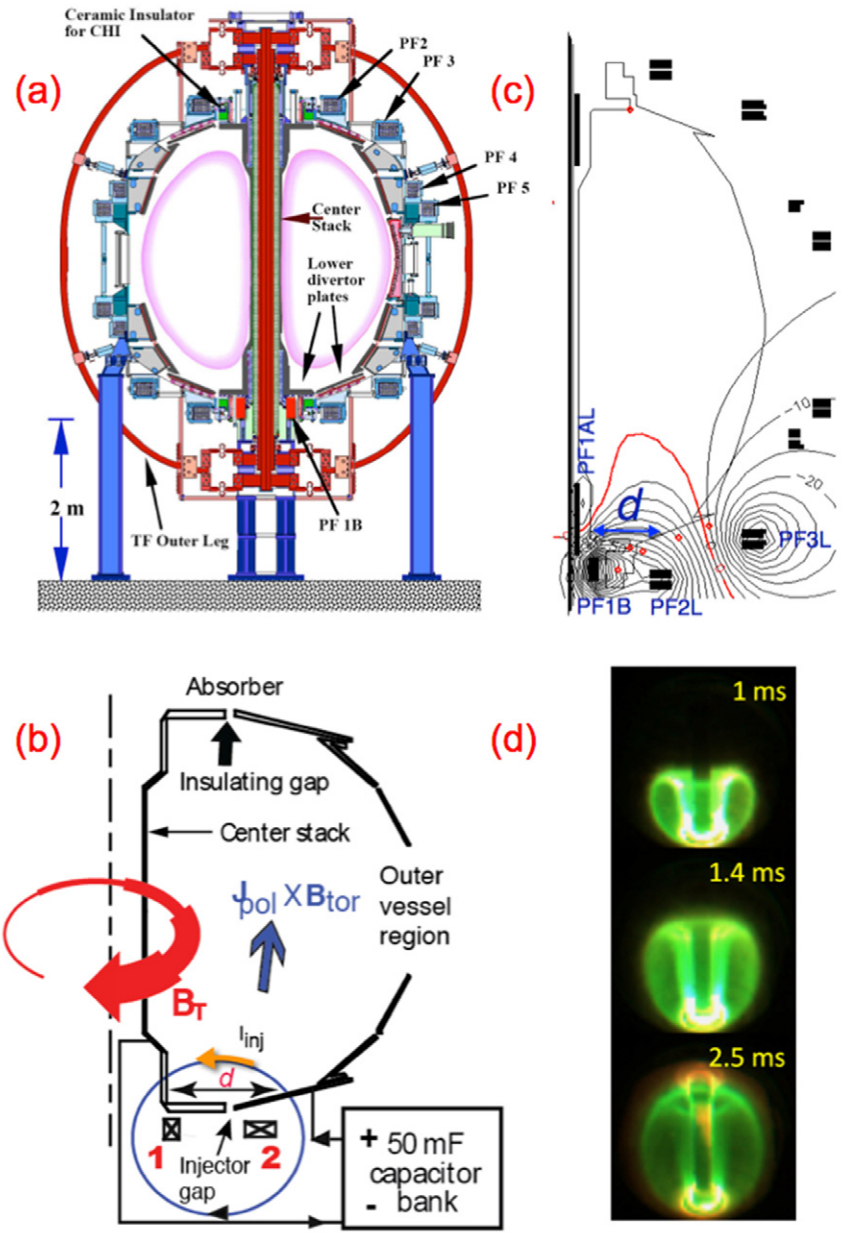

Figure 2. Shown are (*a*) drawing of the NSTX machine, reproduced with permission from [31], (*b*) cartoon of CHI start-up. The coil labeled 1 is equivalent to the PF1B coil that generates the injector flux, reproduced with permission from [43], copyright 2011, AIP Publishing LLC, (*c*) vacuum field line contours of the injector flux for a NSTX CHI start-up scenario. The other nearby coils PF1AL, PF2L and PF3L are used to shape the injector flux generated by the PF1B coil so that the injector flux footprint width '*d*' shown by the arrow is not too wide, and (*d*) fast camera images of an evolving CHI discharge in NSTX 1 ms, 1.4 ms and 2.5 ms after discharge of the CHI capacitor bank, reproduced with permission from [43], copyright 2011, AIP Publishing LLC.

2.1. Transient CHI

CHI is a method in which voltage is applied to electrically insulated coaxial electrodes connected by magnetic flux. CHI on HIT-II and NSTX is achieved by driving current along field lines that connect the inner and outer vessel components on the lower part of the machine [30]. Figure 2 shows a cross-section of the NSTX device, and a simplified schematic of CHI in NSTX [31]. CHI is implemented by injecting current through the plasma from an external circuit along PF lines that connect the lower divertor plates in the presence of toroidal magnetic field. Electrical insulation of the divertor plates is achieved by employing toroidal insulators. In the NSTX and HIT-II devices, there are two toroidal insulators, one at the top and the second at the bottom of the machine, which, electrically separate the inner and outer vessel components. NSTX uses the lower divertor plates as the injector. The opposite end consisting of the upper divertor plates is referred to as the absorber because the $E_{\text{poloidal}} \times B_{\text{toroidal}}$ plasma drift, when voltage is applied across the vessel components, is away from the injector region and into the absorber region. The initial PF connecting the inner and outer divertor plates in the injector region, known as the injector flux, is produced using the lower divertor coil, as qualitatively shown in figures 2(*b*) and (*c*). Increasing the current driven in this coil, which during CHI

application is referred to as the injector coil, increases the amount of injector flux connecting the lower divertor plates. Adjacent coils located on either side of the injector coil are used to shape the injector flux footprint on the divertor plates. A capacitor bank connected across the lower divertor plates is used to drive the injector current.

For plasma start-up, the poloidal injector flux that initially connects the lower divertor plates must be injected into the machine. To achieve this, the injector current must exceed a threshold value, so that the resulting $J_{\rm pol} \times B_{\rm tor}$, stress across the current layer exceeds the field line tensile stress of the injector flux. In CHI terminology, this minimum threshold current is referred to as the bubble burst current and can be shown to be approximately given by the relation [28]

$$I_{\rm inj} = 2\psi_{\rm inj}^2/(\mu_0^2 d^2 I_{\rm TF}) \qquad (2)$$

Here, d is the width of the injector flux footprint on the electrodes and $I_{\rm TF}$ is the current through the center leg of the toroidal field coil. It is important to note that for a single field line connecting the inner and outer divertor plates, as shown in figure 2(*b*), the parameter '*d*' is the distance between these two points on the divertor plates. However, in reality, the injector flux footprint is spread out over much of the divertor plates, as shown in figure 2(*c*), which is a simulated vacuum flux plot for a CHI discharge. In this case the parameter '*d*' depends on the field lines along which the bulk of the injector current flows. Field lines located at larger radius would be longer and will have a higher resistance and less injector current would flow along these field lines. Those that connect the divertor plates near the injector gap would have a much shorter length and also have a higher magnetic flux density, so these would have lower resistance and carry a much larger portion of the injector current. Thus the parameter '*d*' is a measure of how close the oppositely directed field lines are, and this can be controlled by driving current in the nearby PF coils to either increase or decrease the effective injector flux footprint width. An example of this parameter being dynamically changed during a long-pulse CHI discharge on NSTX is shown in [30, figure 4]. On HIT-II, it was empirically determined [32] that the injector current was about 1.5 times the value predicted by equation (2). As the injected current flows along the injector flux, the combination of the toroidal field and the injector PF results in a spiraling field line structure. This is the initial process that produces the toroidal current, measured by the plasma current Rogowski coil. The CHI-produced toroidal current initially flows on open field lines. Relaxation or other reconnection processes are then necessary to produce current that can flow along closed field lines. The images on figure 2(*d*), which are fast camera images from a NSTX transient CHI discharge, show the growth of this plasma, during the first few milliseconds after the capacitor bank discharge is initiated. It shows the discharge fully filling the vessel with about 200 kA of closed flux current [33].

Once the initial magnetic bubble has filled the vessel, CHI can be applied in two different ways. In the first method, after the plasma fills the vessel, the current along the open field lines is continuously driven keeping the open field lines stretched. In this approach know as *driven* or *steady-state* CHI some form of non-axisymmetric magnetic activity is needed to generate current flowing on closed field lines. This approach is attractive from the point of driving continuous steady-state current for sustaining the plasma discharge, and was the first approach used on NSTX [30] and on HIT-II [34]. However, because of excessive radiative losses from the plasma, it was found that currents generated by this approach could not be usefully coupled to the conventional inductive drive, which is used as a measure of the quality of the start-up plasma discharge. Due to its attractiveness for steady-state CD the steady-state approach continues to be investigated using CHI on the HIST device in Japan [35], as well as on the HIT-SI device at the University of Washington, in which a steady-inductive means is used to inject steady-state helicity [36]. This topical review paper on plasma start-up research in STs will not discuss methods related to steady-state current sustainment.

In the second approach, known as *transient* CHI, the size of the capacitor bank power supply is chosen such that on the time scales required for the plasma discharge to fill the vessel, the stored energy in the capacitor bank is depleted. If the injector flux foot print width '*d*' on the divertor plates is sufficiently narrow, then the expanding CHI discharge disconnects from the injector region forming closed flux surfaces. The entire process takes less than 3 ms on NSTX, and less than 1 ms on HIT-II, as shown by figure 3, which are examples of transient CHI-generated discharges from HIT-II and NSTX [37]. The higher plasma current trace for the NSTX discharge has a faster current decay time due to impurity injection as a result of contact of the growing plasma bubble with the upper portion of the machine, which causes some of the injector current to flow along the surface of the upper insulator in a condition known as absorber arc, which can introduce impurities into the plasma. These conditions are better controlled for the lower current discharge. Increased levels of magnetic buffer field from the upper divertor coils and improved conditioning of the upper divertor plates are methods to control these absorber arcs [8]. The maximum current multiplication factor defined as the ratio of the CHI-produced plasma current to the injector current is about 60 for NSTX discharges, compared to 6 in the smaller HIT-II experiment. The current multiplication factor is given by the relation, $\mathrm{CM} = (\frac{\phi_{\rm toroidal}}{\psi_{\rm poloidal}})$, which explains the reason for the higher current multiplication factor in larger devices. For a given injector flux, the generally higher toroidal field in combination with a larger poloidal cross-section results in a higher value of the toroidal flux.

The process was believed to be similar to 2D reconnection, as the generation of closed flux surfaces could be reproduced using the 2D axisymmetric code TSC [38]. More recent simulations using the 3D resistive MHD code NIMROD, provides further confirmation that the process has resemblance to 2D Sweet–Parker type reconnection, and that 3D effects appear to be quite small [39, 40]. These NIMROD simulations show that as the injector current and voltage are rapidly reduced, a toroidal electric field is generated in the injector region. This results in a $E_{\rm toroidal} \times B_{\rm poloidal}$ drift that brings oppositely directed field lines in the injector region closer together, allowing them to reconnect and generate a closed field

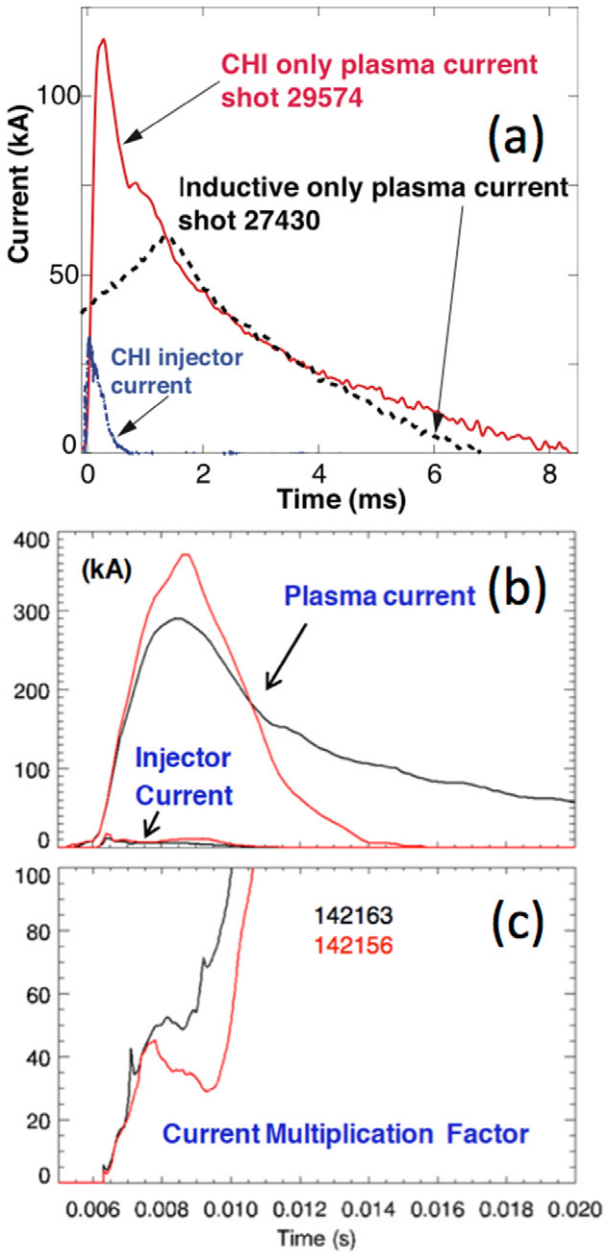

Figure 3. Transient CHI discharges from HIT-II and NSTX. (*a*) Injector current and CHI-generated plasma current from a HIT-II transient CHI discharge. Note that after 0.8 ms, the injector current is zero. All of the left over plasma current of about 60 kA is now flowing on closed field lines. The current decay rate of CHI-produced plasma current is compared to the current decay rate of a similar level of current generated using induction from the CS, showing that the CHI-produced plasma quality is similar to that produced with conventional inductive drive, reproduced with permission from [37]. (*b*) Injector and plasma current traces for transient CHI discharges generated on NSTX, reproduced with permission from [33]. (*c*) The current multiplication factor defined as the ratio of the CHI-produced plasma current to the injector current is about 60 for NSTX discharges, compared to 6 in the smaller HIT-II experiment.

line configuration. A narrow injector footprint width reduced the time needed for these oppositely directed field lines to come together, while a more rapid reduction of the injector current and voltage increases the magnitude of the induced toroidal electric field, both of which are desirable for increasing the closed flux fraction [41]. An aspect of CHI plasma generation using this method is that flux closure can be demonstrated unambiguously by the persistence of plasma current after the injector current has been reduced to zero [42]. On NSTX, when inductive drive is applied to these discharges, it was found that they developed up to 300 kA of additional current compared to what was possible by induction alone [43]. These inductively ramped discharges, on NSTX, have also transitioned to H-mode discharge showing that CHI has generated clean plasmas for plasma start-up purposes and is compatible with high-performance ST operation [44].

The stored capacitor bank energy needed for a transient CHI discharge formation on NSTX is quite small, on the order of 25 kJ. It is necessary that this energy be sufficient both to ionize and heat the injected gas to achieve significant electron temperatures as well as exceed the inductive stored energy in the resulting plasma. NSTX transient CHI discharges use the same level of gas injection as that in the normal pre-fill for standard inductive discharges so that energy needed for ionizing and heating gas is considerably less than the stored capacitor bank energy. An additional requirement relates the maximum final toroidal plasma current I_p that can be produced to the energy available from the capacitor bank: $0.5L_pI_p^2 < E_{cap} = 0.5CV^2$. This sets the limits on the capacitor bank stored energy requirements for generating a given amount of plasma current. Transient CHI discharges on HIT-II and NSTX have reached 30 eV electron temperatures [45]. Future experiments on the NSTX-U device plan to heat the CHI discharges using 28 GHz, 1 MW of ECH power [46], which is predicted to increase the electron temperature to over 200 eV.

The maximum toroidal current generated by CHI is given by the relation [28]

$$I_{\text{toroidal}} = I_{\text{inj}} \left(\frac{\phi_{\text{toroidal}}}{\psi_{\text{injector}}} \right) \tag{3}$$

As described above, the maximum toroidal current generated by CHI can be expressed as the product of the maximum current multiplication ratio and the externally driven injector current. However, the injector current cannot be arbitrarily increased to attain a higher toroidal current. Generally, the injector current is clamped at or near the bubble burst current limit, which is a function of the magnitude of the injector flux, the injector flux footprint width, and the total coil current generating the toroidal field (equation (2)). Substituting equation (2) for the injector current into the expression (3) yields an expression for the maximum toroidal current from CHI. It can be seen that this current is linearly proportional to the injector flux magnitude, and independent of the toroidal field; scalings that have been experimentally confirmed on the HIT-II device [32]. Note, however, increased toroidal flux is useful because it decreases the amount of injector current corresponding to any particular values of toroidal current and injector flux. Reducing the amount of injector current is quite important for any dc helicity injection technique, as it reduces the current density at the electrode surfaces, thereby reducing the incidence of sputtering at the electrode, and producing a cleaner discharge.

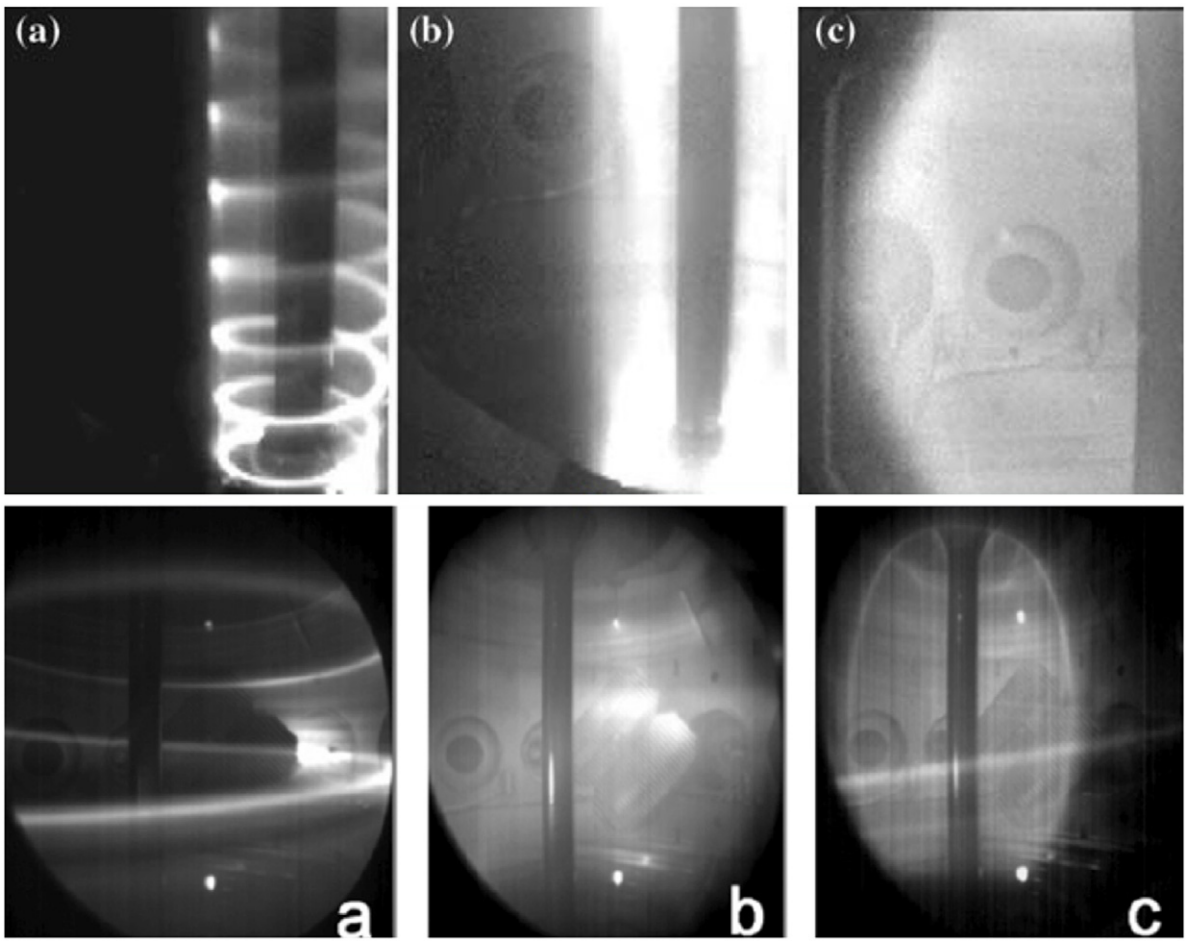

Figure 4. (Top) shown are the spiraling filament structure from an early gun injection experiment on Pegasus in which the gun was positioned at smaller major radius, close to the center stack. (*a*) Filamentary structure during the early phase, (*b*) during filament merging and (*c*) during relaxation to form tokamak-like plasma, reproduced with permission from [9]. (Bottom) similar traces from more recent experiments on Pegasus with the guns positioned near the outer edge of the plasma, reproduced with permission from [55].

Thus the maximum closed flux current that can be generated by a transient CHI discharge is primarily determined by the amount of poloidal flux that can be injected into the vessel. It is because, in the absence of any dynamo activity, it is this flux that eventually reconnects at the injector region to generate a closed flux configuration. The scaling of injected poloidal flux with the CHI-generated toroidal current is also seen in simulations using the TSC and NIMROD codes [38, 41, 47]. In NSTX transient CHI discharges, a large fraction of this injected flux is retained as closed poloidal flux in the resulting discharge [43]. Thus far on NSTX, 50 mWb of poloidal flux has been injected, resulting in closed flux plasma currents of about 200 kA. On the NSTX-U device, to begin operation early in 2015, the capability of the injector flux coil has been increased so that considerably more than 200 mWb of poloidal flux can be injected [4], which is expected to significantly increase the start-up current magnitude on NSTX-U.

2.2. Local helicity injection

While the method of CHI drives current along field lines connecting large surface area electrodes, in the method of LHI, current is driven along field lines that connect a much smaller electrode (usually an active plasma source, providing a virtual cathode for the injector current) that is biased with respect to an anode. The anode could be a discrete electrode or a component of the vessel. The magnetic field lines that connect both these electrodes are generated by external outboard PF coils and the toroidal field coil. The combination of both these fields produces a spiraling field line structure. Plasma flowing along these field lines is shown in figure 4, which are 'fish eye' visible images of Pegasus LHI discharges obtained using a fast framing camera. These field lines connect the active plasma sources to a current return plate.

The relatively small cross-section of the injectors in the LHI strongly constrain the rates of helicity and power injection, relative to CHI. Forming a discharge and building up poloidal flux and toroidal current to particular target values using LHI will necessarily require the injector to be immersed in the plasma edge, injecting helicity and power, for significant intervals of time. This relatively slow evolution permits significant current diffusion in the tokamak during the current buildup, enabling operational 'tuning' of the current density profile [48]. On the other hand, a key consideration for any proposed injector is its capability to sustain kilovolt-scale

injector voltages during the injection phase, while minimizing sputtering and other plasma–material interactions.

The first experiments to test this concept were conducted in the ACT-1/CDX experiment at PPPL [29], where a 50 A electron beam was injected from a cathode at the bottom of the machine to a limiter which was maintained at the vessel potential. The cathode was composed of heated lanthanum hexaboride (LaB_6), about 1 cm in diameter that was placed on top of heated carbon rods. LaB_6 was used for its high emissivity at low temperature. These experiments were further improved on the larger CCT tokamak [49], at UCLA, where up to 6 kA of toroidal current was generated [50]. The work was later extended to the low aspect ratio CDX-U [51] device at PPPL. Since those early experiments, to allow greater electrode current densities, the technology required for electron beam based plasma start-up was considerably improved by the Pegasus group at the University of Wisconsin, which has now demonstrated the primary aspects of significant current generation, as well as coupling that current to conventional inductive drive [9].

Early LHI experiments on Pegasus used two active-arc injectors located in the lower divertor region, with an anode plate covering the upper divertor. Each of these arc injectors, described in [52, 53], consists of a discharge channel formed by a stack of alternating conducting and insulating washers, with a deuterium gas feed located behind the channel. Each arc injector has a separate power supply to drive the arc in this channel, with the arc cathode being the 'cup' with the gas feed and the anode being the last conducting washer in the stack. The stack of washers have the effect of evenly grading the arc-driven electric field in the channel, and the channel should be approximately aligned to the externally generated magnetic field for optimum operation. For a given toroidal field the PF must be large enough that the plasma stream does not strike the back of the gun after one toroidal transit.

The top three images in figure 4 show the time evolution of an LHI discharge from these early experiments, progressing from left to right. The first image shows plasma streams from the arc injectors, with no injector current, so that the streams simply follow the helical vacuum field. The second image shows the merging of the helical streams and initial formation of a (highly elongated) low-current tokamak, after significant injector current has been applied. The third image, after injector shutoff, shows the relatively high-current tokamak equilibrium remaining after a drive period of several milliseconds. These active-arc injectors can drive injector current with density up to $6\,\mathrm{MA\,m^{-2}}$, with low impurity content, as long as the extracted injector current is significantly less than the arc current (typically 2–3 kA). Under this condition, the vast majority of the current is extracted from the virtual cathode of the plasma arc, rather than from the metal surface of the plasma gun. This can be understood as follows. Typically in arc discharges, the arc occurs across two metal electrodes. Under this operating condition, ions bombarding the metal cathode can sputter impurities into the plasma discharge. With the active-arc injectors (plasma guns) used on Pegasus, a plasma arc generated inside the gun protects the metal cathode. By driving a current between this plasma arc (the virtual cathode) and the external anode sputtering can be significantly reduced as long as the injector current for plasma start-up is less than the arc current flowing internally within the gun source.

More recent Pegasus experiments have used an array of three active-arc sources located 0.2 m below the outboard mid-plane of the device, with the corresponding anode (a 'button' limiter) located 0.2 m above the mid-plane, at the same toroidal location. The lower three images in figure 4 show the evolution of a discharge driven by the outboard injector array, progressing from left to right. The first image shows the arc plasma streams following the helical vacuum field, the second shows the diffuse light emission of the driven state (in which the injector-driven current streams are no longer clearly visible), and the third shows the tokamak equilibrium resulting when the injector current is reduced to zero. The arc plasma streams are again visible in the third image, though they are quite dim with respect to the tokamak equilibrium. A key advantage of outboard injection is that the plasma evolution, from a small outboard-limited initial discharge to one that finally fills the confinement region, takes advantage of the effective inductive drive associated with the changing plasma inductance and any increases in the vertical field. This effective inductive drive is on the order of volts, and can significantly enhance plasma performance relative to the early divertor-injection experiments [9]. On the other hand, the inductive drive associated with the vertical field is quite significant, to the point that development of an outboard-injection operating scenario can be complicated.

The physics of helicity injection for LHI is similar to that for CHI. The LHI maximum current has been derived in terms of the localized injector geometry, the injector current and the toroidal field coil current, but this expression can be recast in a form that is nearly identical to that for CHI given above. As with CHI, the energy per unit helicity of the injection region must exceed that in the confinement region so that helicity can flow from regions of high λ to regions of lower λ. Here the average edge λ is given as $\lambda_{\mathrm{edge}} = \mu_0 I_{\mathrm{inj}}/\psi_{\mathrm{edge}}$. The edge flux is given as $2\pi w B_{Z-\mathrm{edge}}$ The injector current is that which flows in an axisymmetric sheet of poloidal flux of width w between the gun, which is the cathode at radius R_{gun}, and the anode. The λ of the tokamak plasma, is given as $\lambda_{\mathrm{p}} = \mu_0 I_{\mathrm{p}}/(A_p\langle B_\phi\rangle)$. Here the denominator is the toroidal flux enclosed by the tokamak plasma, which is given as the product of the plasma cross-sectional area and the average toroidal field in that region. The maximum value I_{p} could have is dictated by the Taylor relaxation limit. This places an upper limit on the generated toroidal current given as [54]

$$I_{\mathrm{p}} \leqslant f_{\mathrm{G}} \left[\frac{\varepsilon A_{\mathrm{p}} I_{\mathrm{TF}} I_{\mathrm{inj}}}{2\pi R_{\mathrm{gun}} w}\right]^{0.5} \tag{4}$$

where ε is the inverse aspect ratio, A_{p} is the plasma cross-sectional area, I_{TF} is the total TF coil current, I_{inj} is the injector current, R_{gun} is the radial location of the injector(s), w is the width of the driven edge, and f_{G} is a dimensionless geometric function on the order of unity (the exact value of f_{G} depends upon the plasma geometry, varying from 1 in the limit of

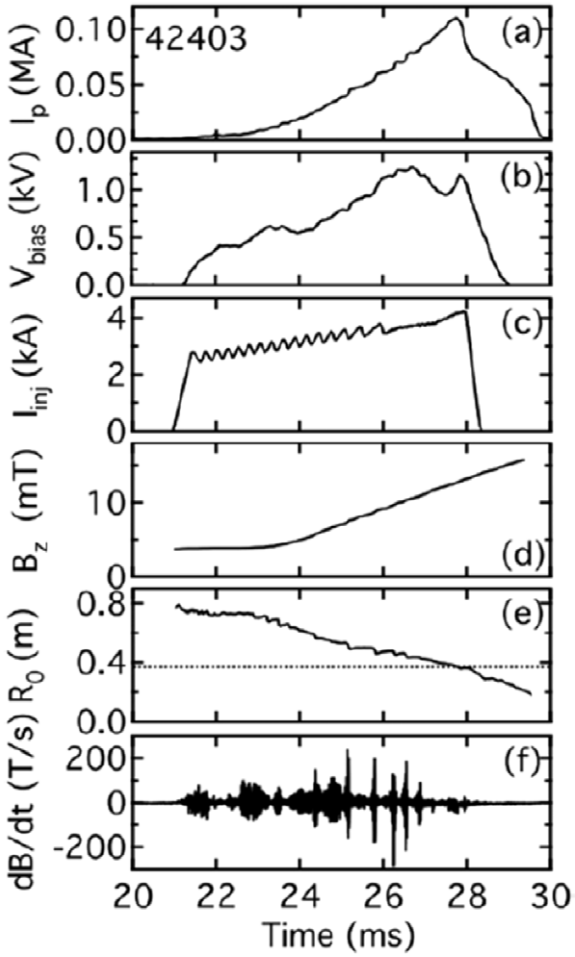

Figure 5. From top to bottom, shown are traces of the plasma current, gun bias voltage, the injected gun current, vertical magnetic field at the machine major radius, estimated major radius location and dB_z/dt near the outboard mid-plane, reproduced with permission from [55].

large aspect ratio and circular cross-section to approximately 3 in typical Pegasus geometry). Experiments on Pegasus have achieved plasma currents that are a high fraction of the theoretical relaxation limit [54].

The injector current is analogous to that for CHI. In both cases, the injector current is driven along field lines that connect electrodes. After the initial formation of the tokamak-like state, the injector current is maintained, with corresponding high injector voltage, so that helicity and power are injected at a rate greater than resistive dissipation, allowing the toroidal plasma current to increase while the injection is sustained. Time traces from an example outboard-injection Pegasus discharge are shown in figure 5 [55]. In this particular discharge, approximately 4 kA of injector current enables formation of toroidal current of 0.10 MA. More recent Pegasus results use 4–6 kA to form discharges with currents up to 0.18 MA. After the injector current rapidly drops to zero, the plasma current also begins to drop, partially due to the lack of CD and partially due to being crushed into the central column as the vertical field continues to increase after the injector current drop. However, much of the plasma current persists, indicating that closed flux equilibrium has been generated. Such LHI-generated start-up plasmas can be driven inductively using the CS, and the current ramped up still further and sustained to the end of the inductive drive [56].

As expected, the calculated plasma major radius shows that the discharge is initially small and forms near the injector radius, and that the plasma both grows and moves inward as the plasma current increases. During the helicity injection phase, LHI plasmas exhibit robust MHD activity, which is generally incoherent in the early phase of the discharge but can later be resolved as coherent bursts with $n = 1$ structure. This is analogous to the $n = 1$ activity that has been seen in driven CHI discharges [34], which suggest that these plasmas have some connection to steady-state CHI discharges.

Recent simulations using the resistive MHD code NIMROD show that adjacent turns of the helical injector-driven current stream will be attracted together, prompting highly localized reconnection between these parallel current paths and the formation of axisymmetric current rings [57, 58]. In the context of these simulations, each burst of MHD activity observed in the experiment corresponds to an instance of reconnection, and the formation of another axisymmetric current ring, which merges with other such rings to form the core plasma. This simulation work has motivated a closer collaboration with the Pegasus experimental group, with the goal of developing detailed tests of the physical scenario described by the NIMROD simulations.

For a particular toroidal field, it can be seen from equation (4) that increasing the maximum plasma current I_p will require increasing the injector current I_{inj} while minimizing the width w of the injector-driven region. The helicity injection rate, proportional to the product of injector voltage and injector cross-sectional area, is proportional to the effective toroidal loop voltage of the LHI CD. Achieving high LHI current will require both a high Taylor limit and high effective loop voltage. To satisfy these conditions, the Pegasus group has recently explored alternative injector technologies, including large-area passive electrodes (constructed from molybdenum and carbon) and large-area gas-fed active electrodes (for a distributed hollow cathode effect). These large-area electrodes have been found to have remarkably small effective cross-sectional areas, primarily due to the tendency of physical electrode surfaces to break down into sub-millimeter cathode spots at large injector currents [59]. These results prompted a renewed interest in active-arc injectors, especially improvements that significantly increase the injector voltage standoff capability. These developments will be incorporated into a larger scale test of the LHI start-up concept on the NSTX-U device.

An advantage of LHI is that the guns could be withdrawn, after plasma formation. As a future step to both CHI and LHI concepts, design studies and scenario development are needed to determine optimum location of insulators for CHI based systems, optimum location for LHI injectors, and feasible techniques for extracting LHI injectors during non-inductive current ramp-up using neutral beams and RF waves to reach currents required for sustained ST operation.

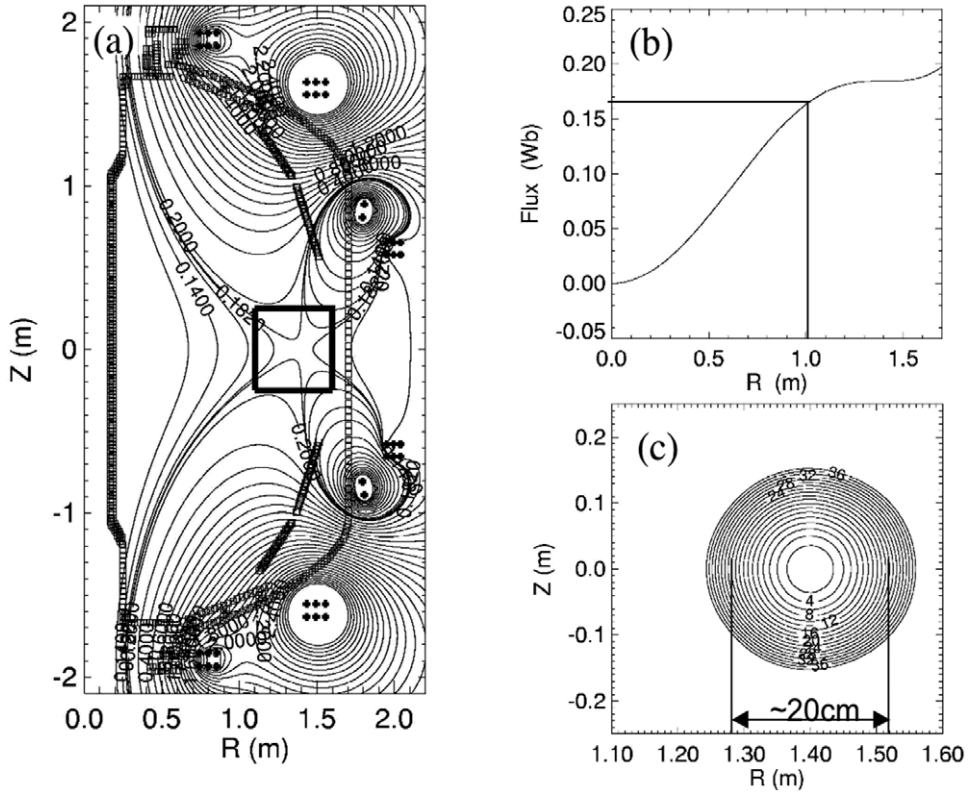

Figure 6. The NSTX null-field configurations: (*a*) flux contours [Wb]; (*b*) flux radial profile; (*c*) Mod-B [Tesla$\times 10^{-4}$] surface of the field null region.

3. Start-up using induction from outer PF coils

3.1. Induction from outer PF coils

This method uses the external PF coils to induce a toroidal electric field inside the vessel to generate the plasma current. The basic concept of plasma start-up with outer poloidal coils is described here using simulations, shown in figure 6, that were conducted for the NSTX device, in which the PF coils are located outside the vacuum vessel [60]. There are three important conditions that need to be satisfied for this form of inductive start-up [61].

(1) In general, a region of low poloidal magnetic field must be created over a sufficiently large region of the vacuum vessel poloidal cross-section to allow the ionization avalanche to develop in the applied toroidal electric field. The condition for highly reliable breakdown can be expressed as $E_T \cdot B_T \,/\, B_P > \sim 1\,\mathrm{kV\,m^{-1}}$, where E_T is the induced toroidal electric field, B_T is the toroidal magnetic field and B_P is the average poloidal (i.e. transverse) magnetic field. This is generally referred to as the Lloyd condition [62]. However, the application of suitable RF waves to break down the gas can significantly relax this condition, to the extent that the region of low poloidal magnetic field is no longer essential. For example, on DIII-D, operating at $B_T = 2\,\mathrm{T}$, with high-power ECH pre-ionization ($\sim$800 kW), start-up was achieved at $E_T = 0.3\,\mathrm{V\,m^{-1}}$ with $B_P > 5$ mT over most of the vessel cross-section [62]. This represents a value of $E_T \cdot B_T \,/\, B_P \approx 0.12\,\mathrm{kV\,m^{-1}}$. Calculations for NSTX start-up suggest $E_T \cdot B_T \,/\, B_P \sim 0.12\,\mathrm{kV\,m^{-1}}$, but without the benefit of high-power ECH.

(2) The field null, which is produced transiently by the combined effects of currents in the PF coils and the induced currents in the machine structure, must be maintained for a sufficient duration, typically $\sim$3 ms to develop the avalanche. DIII-D experiments found that the time required increased as the loop voltage was reduced. However, high-power ECH pre-ionization ($\sim$800 kW) was able to shorten this process on DIII-D to $\sim$2 ms even at low loop voltage. It is useful to note that the currents in the outermost PF coils are initially opposite in direction to that required for the final closed flux equilibrium, so these coils should be designed to handle the high-current ramp rates that allows the coil current polarity to be reversed on these short time scales.

(3) After breakdown, the PF coils must provide both fields to maintain plasma equilibrium and sufficient flux change for the current to ramp up to the desired level. The change in the vertical field required for equilibrium produces additional flux during the current ramp-up. As part of this requirement, it is necessary that the field pattern must be radially and vertically stable. For example, in recent experiments on DIII-D it was found that until the vertical field's index of curvature was radially stable, the plasma produced by the loop voltage was lost until it became stable [14]. Although there was visible light, there was little current, and the current did not ramp-up until it was positionally stable.

Figure 6(*a*) illustrates the results of vacuum field calculations using only the outer PF coils, which show the resulting two-dimensional PF contours. The currents in the coils have been adjusted to create a region of large field null, shown by the small square region located near $R = 1.4$ m. From Figure 6(*b*), one can see that about 0.16 Wb (at $R = 1.0$ m) is available for the current ramp up for this particular set of coil currents. In NSTX, under an optimized condition, about 0.3 Wb from the solenoid can produce a 1 MA discharge. Thus, the 0.16 Wb flux swing available from this scenario at $R \approx 1.0$ m could, in principle, produce plasma currents of order 0.5 MA. However, NSTX lacked high-power ECH to adequately test the concept, but nevertheless was able to generate about 20 kA of plasma current. In addition, in the configuration that could supply the most flux, the plasma was radially unstable and failed to produce any current.

Both DIII-D and JT-60U are equipped with high-power ECH systems and were both able to generate about 100 kA of plasma current using the outer PF coils. On JT-60U, high-power ECH pre-ionization in combination with a flux swing from four outboard PF coils was able to generate 100 kA using a region of large field null as described in the context of figure 6. About 85 kA of plasma current was also generated without the presence of any field null. In this case the same four coils were initially pre-charged to contain negative current and the coils rapidly ramped up in current as shown in figure 7. The initial vertical field, before start of the flux swing, is opposite that required for plasma equilibrium. 1 MW of ECH at 110 GHz was sufficient to achieve significant breakdown and the resulting flux swing sufficient to generate the plasma current [15]. Efficiency, as could be expected, was lower than for the case with some field null. A flux swing of 3.1 Wb was needed to produce 85 kA, compared to 1.3 Wb for the case with the presence of a field null that generated 100 kA plasma current.

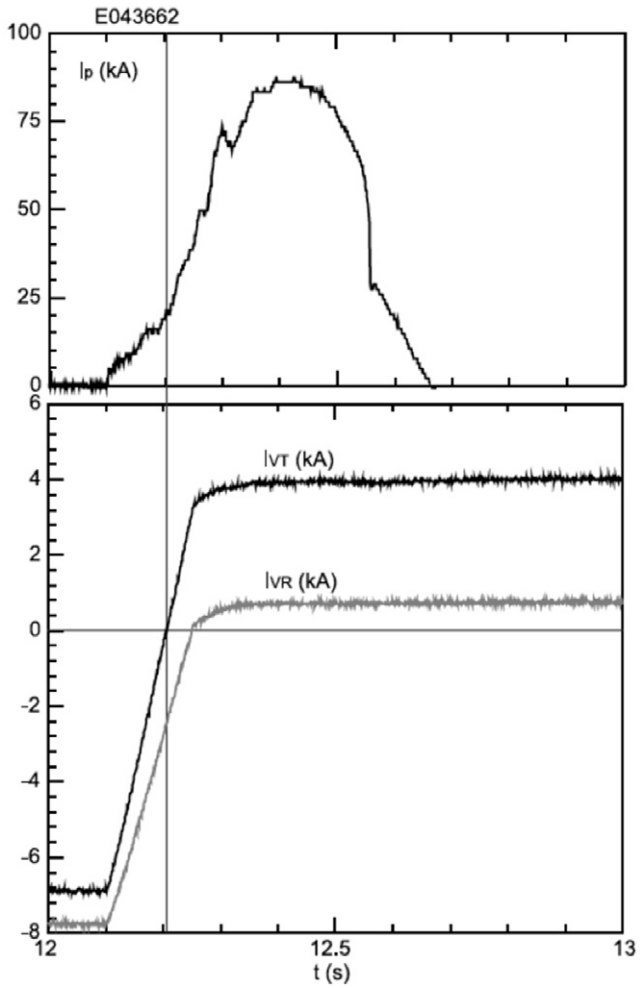

Figure 7. CS-less start-up in JT-60U without the presence of a field null. The two VR coils are the two largest in radius outboard mid-plane coils located above and below the mid-plane. These are the primary coils that generate the vertical field for plasma radial equilibrium. The VT coils are the ones just above and below the VR coils and at slightly reduced major radius, reproduced with permission from [15].

3.2. Merging compression and double null merging start-up

These methods were first developed on the START device and then have been successfully employed on MAST. These methods also rely on the use of the outer PF coils, but program them differently to generate two rings of plasma that then reconnect and merge to form a tokamak-like plasma. In both these devices the PF coils are located inside the vacuum vessel. The MAST experiment used PF coils at a larger major radius than the plasma but still inside the vacuum chamber to initiate the plasma. However, to be able to extrapolate this technique to future experiments, and fusion energy systems, it would be advantageous to use only the PF coils located outside the vacuum vessel wall for start-up. This is being studied and developed on the UTST device in Japan.

Merging compression start-up is described using figure 8, which show the poloidal coil locations on MAST. To begin the discharge, after energizing the TF coil, followed by pre-fill gas injection, the P3 coil current is ramped up in current to a high level, and then rapidly ramped down. This results in breakdown in the form of plasma rings around each of the P3 coils. The current in both these rings is in the same direction, which causes the rings to attract and merge at the mid-plane [6, 10]. The vertical field coils P4 and P5 coils are used to compress and shape the plasma into the required configuration. If the resulting discharge is not compressed in this manner, the process is referred to as merging-reconnection start-up. Formation of the rings near the P3 coils at 0.7 ms, and full merging that results by 8 ms are shown in the sequential fast camera visible images in figure 9. The current generated during this process is shown in figure 10 and compared to that obtained during normal inductive start-up using the CS. The generated plasma current ramps up to 400 kA within 10 ms. The slow gradual current decay of the resulting currents indicates the formation of a high electron temperature discharge.

During double null merging compression, a ring plasma is formed in the region between the P2 and P3 coils, by driving high current in these coils and then reversing the currents in these coils. The method is easier to implement in devices in which the coils are located outside the vessel as the ring plasmas that form are between the two coils, so this region could be inside the vacuum vessel. Figure 11 shows results

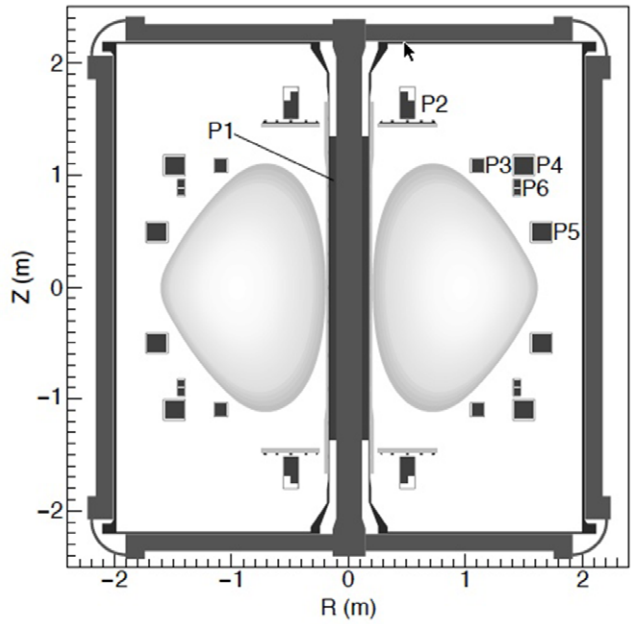

Figure 8. Poloidal coils configuration in the MAST device, reproduced with permission from [10].

from such a discharge on the START device. The discharge initially forms in the top and bottom, corresponding to the label 'A' in the plasma current trace. These merge on about a millisecond time scale to a tokamak-like configuration by 2.75 ms, corresponding to location 'D' in the plasma current trace [63]. Additionally, in these discharges, the reconnection process also effectively heats the ions. As with outer PF start-up, the effect of the vessel walls on start-up needs to be understood to extrapolate these methods to future devices. This is now being studied in the UTST device [64] at the University of Tokyo.

The UTST stainless steel vessel has a thickness of 1.5 mm. The time constant of current ramps in the PF coils is about 1 ms. This results in a skin depth of 13.3 mm in the SS304 vessel, much more than the vessel thickness of 1.5 mm, which allows the coil fields to easily penetrate into the vacuum region inside the vessel. In these experiments up to 25 kA in ring plasmas were generated, and when merged generated up to 50 kA of plasma current [65]. The resulting discharge at lower levels of start-up plasma current was also coupled to inductive drive using the conventional CS and reached currents up to 140 kA.

As a next step to formation using the outer PF coils, as well as the double null merging scenarios, design studies are needed to understand the current generation potential in future devices in which the coils would be located outside blanket structures.

4. Plasma start-up using RF waves

Several STs are actively involved in developing plasma start-up methods using RF wave injection systems. Other experiments have also contributed to this research in the past. RF methods employed for plasma start-up are based on the use of electron cyclotron (EC), heating LHCD, and more recently, the much more promising EBW CD. These will be described in this order.

4.1. ECH start-up

The necessary requirement for RF wave propagation in plasma is that the wave frequency exceeds the electron plasma frequency $\omega_{RF} > \omega_p$. The electron plasma frequency, $\omega_p = (\frac{n_e e^2}{\varepsilon_0 m_e})^{1/2}$, increases with the plasma density, but the plasma transparency requirement is easily satisfied during the early phase of a discharge as the plasma density is very low. In addition, there must be a fundamental or second harmonic EC resonance layer present somewhere inside the vacuum vessel. The fundamental EC resonance occurs when the RF wave frequency equals to the EC frequency, $\omega_{ce} = eB/m_e$. This depends on the operating toroidal field of the device, so the required wave frequency increases with the device toroidal field. EC resonance heating (ECH) is very effective in heating plasmas at very low electron temperatures, including plasmas with zero electron temperature. Because of this ECH is commonly used as a source of pre-ionization for conventional inductive start-up in several tokamaks.

Physics of inductive and RF breakdown in gas is very similar. In the presence of the inductive or RF electric field the breakdown becomes possible if the ionization rate exceeds the losses. Losses are primarily determined by the gas pressure and characteristic connection length L, which depends on the magnetic field geometry. According to RF break-down theory [66] the breakdown voltage increases with the RF frequency increase due to the fact that the amplitude of electron oscillations becomes smaller and electrons get smaller energy from the electromagnetic field of higher frequency. The effective electric field E_{eff} is often used as a representative value in RF break-down estimates. For deuterium it can be estimated as

$$E_{eff} = \frac{E}{\sqrt{1 + (55.6/p\lambda_{RF})^2}} \approx \frac{p\lambda_{RF}}{55.6}E \qquad (5)$$

where E is an RF electric field, p is the gas pressure in Torr and λ_{RF} is the vacuum wavelength in centimeters. In contrast to the inductive plasma breakdown, in the presence of EC resonance the minimum electric field required for RF breakdown does not depend on L [67]. This fact makes ECH very attractive for plasma pre-ionization and discharge initiation because even in the absence of poloidal null RF power can produce a reliable breakdown. During ECH pre-ionization the inductive electric field is partly substituted by the RF electric field, which results in significant reduction of the solenoid flux used in the plasma start-up.

As described in section 3.1, use of high-power ECH is very effective in reducing the loop voltage requirements for inductive start-up. It is thus an important system in many conventional tokamaks, and will also be used on ITER for this purpose. As described in section 3, the ease with which ECH can be applied has allowed DIII-D and JT-60U to employ it in combination with the inductive loop voltage from the external PF coils to generate 100 kA of start-up current in both devices. It is also planned to be used on the NSTX-U device to increase the electron temperature of transient CHI discharges.

The very earliest test of ECH plasma current start-up in an ST was conducted on CDX-U at PPPL [16]. For purely RF based start-up, the initial condition requires the addition

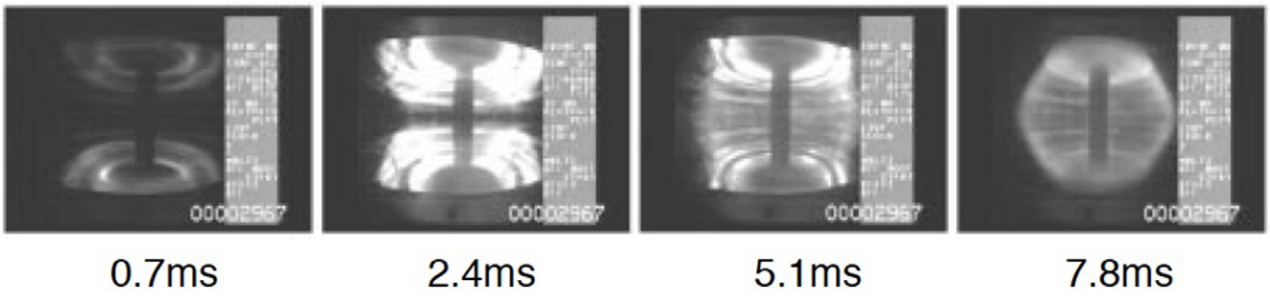

Figure 9. Fast camera visible images showing plasma formation by merging compression in a MAST discharge, reproduced with permission from [10].

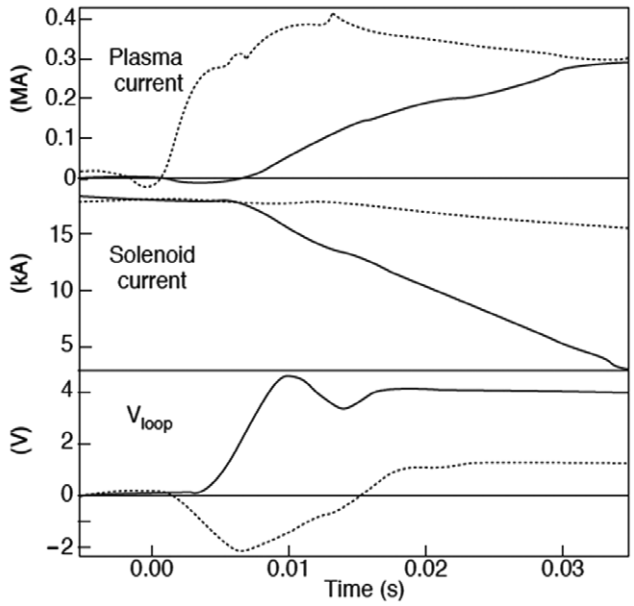

Figure 10. Comparison of plasma current, solenoid current and the generated loop voltage during the merging-compression process, shown by the dotted lines, and during normal inductive operation using the CS, shown using the solid lines. Approximately 4 V is required during standard inductive operations. During the merging-compression process (the first 10 ms) the loop voltage is negative, reproduced with permission from [10].

of a vertical magnetic field, which has a minimum at the mid-plane. The vertical field must be relatively weak so that the combination of this field with the much stronger toroidal field allows for a sufficiently large field line wrap around factor. A small pre-fill gas is then injected, followed by the application of the RF power. Under these conditions, the generated electrons can propagate to the regions of higher toroidal field, where they can reflect back by mirror fields and generate tokamak-like banana orbits.

On CDX-U ($R \leqslant 56$ cm, $A \geqslant 1.3$) [16], typical ST parameters were the toroidal field of 87.5 mT, and the vertical field of about 1 mT in the device center. About 8 kW of the RF power at 2.45 GHz was injected. This generated about 1 kA of plasma current. During the initial phase of plasma formation, the current flows on open field lines, and no closed flux surfaces are present. The authors hypothesized that at this initial open-field line phase, the net current is explained on the basis of toroidal precession of the electrons trapped on the banana orbits. Also during the open-field line phase, the field-aligned currents from the Pfirsch–Schluter effect maintaining quasi-neutrality are in the same direction on the inside and the outside of the plasma. Thus a net toroidal current can add to flux surface closure. Once the sum of these currents exceeds a critical value, such that the PF created by these currents is able to cancel the externally generated vacuum field on the inner side of the plasma current channel, the closed flux surfaces can begin to form, as described below in the more recent experiments on the LATE device. Once the closed flux surfaces formed, then the Pfirsch–Schluter current on the inside cancels the current on the outside, and as a result it cannot contribute to a net toroidal current. However, pressure driven bootstrap current can now start to play a much larger role in increasing the net toroidal current.

On LATE [68] ($R = 50$ cm, $A \sim 1.4$), with a toroidal field of 96 mT at $R = 25$ cm, and a vertical PF of 7 mT, both at $R = 25$ cm, 190 kW of 5 GHz ECH is used. Initially, the vertical field is held constant in time. The plasma discharge is initiated at the second EC harmonic location ($R = 27$ cm), followed by a very rapid plasma current rise. After the toroidal current reaches 7 kA, fast camera images show the prompt appearance of a closed field line structure. The current ramp rate immediately slows down, as seen in figure 12. Starting from this time, the vertical field is ramped up which results in the current further ramping up to about 13 kA. After that the ramp rate of the vertical field is substantially reduced, however, the plasma current continues to ramp up at a substantial rate and reaches 20 kA at the time when the ECH pulse is turned off. The electron density remains nearly constant until 40 ms, then increases by a small amount during the third final phase of the pulse. During the 70 ms pulse only pre-fill gas at a magnitude of 7 mPa was used, and no additional gas was injected. The loop voltage remained near zero during the initial 40 ms, but becomes negative during the third phase of the discharge, suggesting that substantial RF wave CD is a possible contributing factor. Towards the end of the pulse, the electron density is estimated to be about 4×10^{11} cm^{-3}, somewhat higher than the RF wave cut-off density of 3×10^{11} cm^{-3}, suggesting the possibility of EBW CD during this third phase. Electrons with energy of about 100 keV are measured and these energetic electrons dominate the energy content of the plasma.

Recently the LATE group has developed a model for the non-inductive formation of closed flux surfaces during

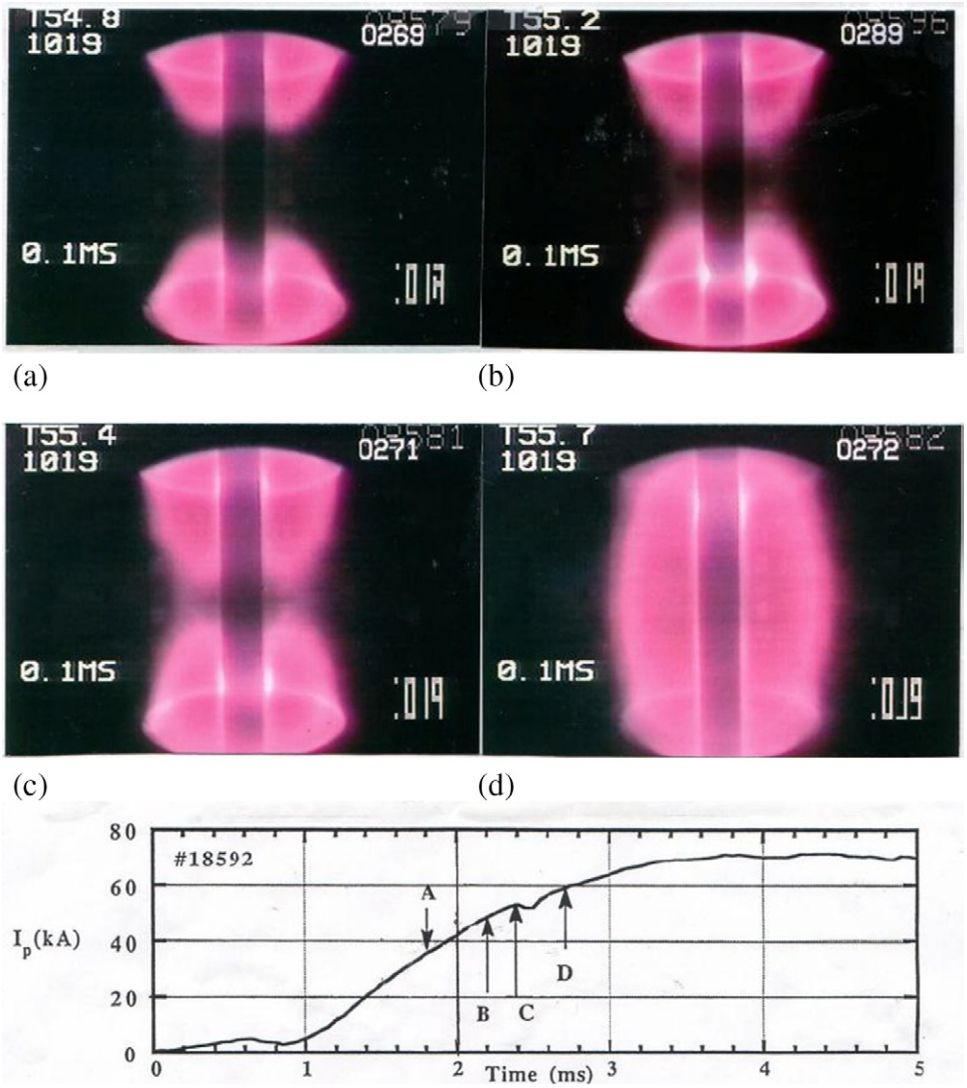

Figure 11. Fish eye visible camera images of an early double null merging discharge on START, with coils located inside the vacuum vessel, and time trace of the plasma current showing the generation of 70 kA of plasma current. The rings merge within 1 ms of formation [63].

RF start-up in STs [69]. The model is based on previously developed two mechanisms of current generation. These mechanisms are a bulk electron-pressure driven equilibrium current and a preferential confinement of energetic electrons. First, in open fields the pressure driven current originates from the vertical charge separation due to the drift of the bulk plasma in the toroidal field. When the self-field from this current is about to cancel the external vertical field inside the current channel the orbits of energetic passing electrons begin to broaden in the velocity space and start making so-called cross-field passing orbits. The electrons occupying these orbits are assumed to be supplied by pitch-angle scattering of the ECH heated bulk electrons. It is then suggested that the cross-field passing electrons provide an additional current that forms closed flux surfaces. Further increase and sustainment of plasma current is attributed to the conventional EC CD.

Current start-up using RF waves are now being extended to much higher power and for much longer durations on the large QUEST ST. On QUEST ($R/a = 0.68/0.4$ m), $B_T = 0.25$ T, 8.2 GHz ECH at a power of about 100 kW was used to generate 35 kA of plasma current. In more recent experiments, 28 GHz second harmonic ECH was used to generate 65 kA in a pulse that was maintained for 1 s at an RF power of <350 kW [70].

Several devices including QUEST, MAST, LATE, TST-2 are actively engaged in understanding the CD mechanisms for RF assisted current start-up in STs and the scaling relations that would allow the start-up currents to be extended to higher levels, and with plasma parameters allowing further transition to the conditions required in a future ST-FNSF.

4.2. LHCD start-up

In tokamaks, LH waves have proven successful for CD with good CD efficiency. LH waves are space-charge waves, which cannot propagate in vacuum. To excite these waves inside the plasma a special phased waveguide array must be used in close proximity to the plasma boundary. To achieve CD, these waves are launched with a specific phase velocity along the magnetic field, and so that they can resonate with electrons with a certain energy. Electrons in the chosen range of energies can then

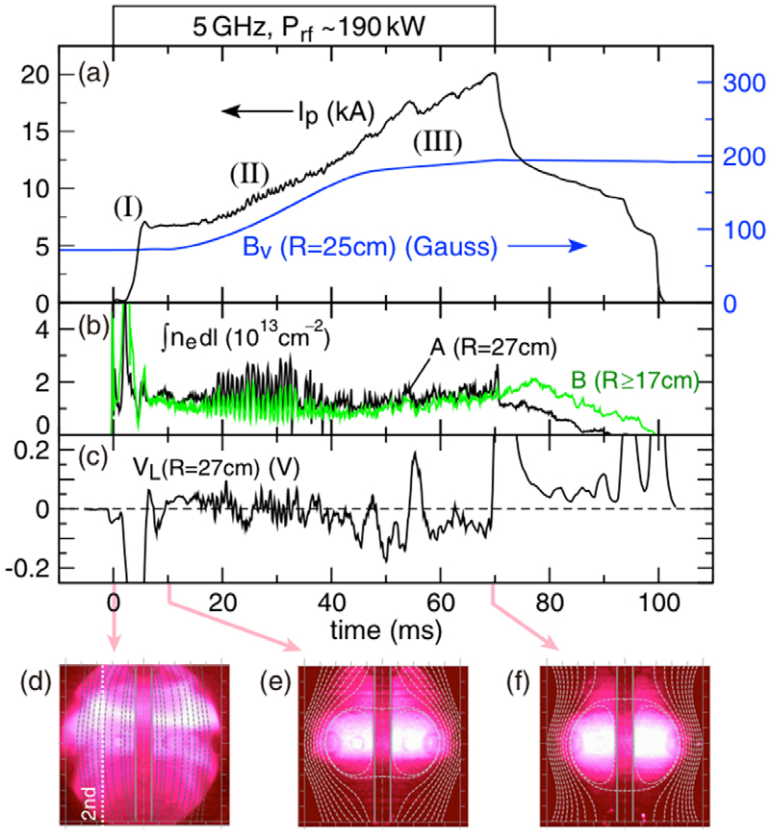

Figure 12. Formation of a 20 kA discharge on the LATE device. (*a*) Plasma current and vertical magnetic field. (*b*) Line densities at two interferometer chord locations and (*c*) loop voltage at the plasma core. Frames (*d*)–(*f*) show the visible images of the plasma during breakdown, initial closed field formation and final low aspect ratio torus formation, respectively [68].

absorb the wave energy through Landau damping processes. These more energetic electrons are now less collisional, so undergo fewer collisions, which aid CD.

On the PLT tokamak ($R = 1.32$ m, $a = 0.4$ m, $B_T = 2$ T), up to 200 kW of LH waves at 800 MHz was used to generate 100 kA of plasma current [21]. The initial vertical field was about 3 mT. Following plasma breakdown, the waveguide phase was adjusted so that the waves propagated toroidally in one direction to drive electron current. The current was ramped up to 100 kA over a period of 2 s. The discharge was initiated with an initial gas pre-fill of about 1.3–2.6 mPa. The initial electron density was about 5×10^{11} cm^{-3}, which rose by about an additional 50% during the 2 s pulse, without any additional gas injection. The measured loop voltage remained below zero during the 2 s discharge. Hard x-ray measurements suggested the current was being carried predominantly by a fast electron tail, and much of the discharge was localized to within a minor radius of about 12 cm. An important experimental aspect of successful CD is careful programming of the vertical magnetic field and its curvature, so that the electrons are accelerated to sufficiently high energy before they are lost on poorly formed flux surfaces.

The low magnetic field in STs in combination with typical densities needed for plasma operation results in a high plasma dielectric constant for LH waves. This fact combined with the high toroidicity typical for low aspect ratio makes the application of this method more challenging in an ST. Extensive numerical modeling of LH wave excitation, propagation and damping was conducted at the University of Tokyo for the low-density plasmas typical during the start-up phase. It was found that effective LH wave core absorption and LHCD are possible in the low-density, low-current fore-plasma specifically formed by ECH [71]. Stimulated by modeling results such an LHCD ramp-up technique is being studied on the TST-2 device using various antenna configurations [72].

In the TST-2 device ($R \leqslant 0.38$ m, $a \leqslant 0.25$ m, $B_T \leqslant 0.3$ T) up to 15 kA of plasma current was generated using <60 kW of LH wave power at a frequency of 200 MHz. All these experiments used 8.2 GHz ECH to achieve pre-ionization and to generate an initial current of about 1 kA by ECH, which is then ramped up using LHCD. Similar results were obtained using two different antennal types, an inductive combline antenna and a dielectric-loaded waveguide 'grill' antenna. A new capacitively coupled combline antenna will be tested in the near future.

Given that future ST based devices are projected to operate at about 2.5 T, the attainment of 100 kA on the PLT in comparison with 15 kA already achieved on the TST-2 at 0.3 T suggests that through improved design of antenna structures needed for the high toroidicity in combination with improved vertical field shaping may allow the higher CD efficiencies, as seen in large aspect ratio tokamaks, to also be realized in STs.

4.3. EBW start-up

Future ST reactors are envisioned to operate at toroidal fields of about 2.5 T. In order to have a fundamental EC resonance inside the vessel, the RF frequency needs to be about 70 GHz, or less for devices with the lower toroidal field. This frequency results in the cut-off density of 6×10^{19} m^{-3}, while the operational plasma density range is projected to be $(7–15) \times 10^{19}$ m^{-3} [73]. In this situation the fundamental EC resonance and its second harmonic will probably be partially or totally obscured by the cutoffs. Fortunately, an interesting opportunity arises from wave–plasma interaction processes allowing the injected electromagnetic wave within the EC range of frequencies to be mode converted into the EBW wave, which has no high density cut-off limit, and is projected to provide substantial CD, as recently demonstrated on the MAST device [74].

EBWs are longitudinal electrostatic waves. Similarly to LH waves they cannot propagate in vacuum. However in contrast to the LH wave the EBW wave can be excited within the plasma by the externally launched electromagnetic wave via various mode conversion mechanisms as described in the Topical Review paper by Laqua [75]. EBWs may propagate into the bulk plasma and may be absorbed near the EC resonance or its harmonics by cyclotron damping. The usual relativistic resonance condition must be satisfied by electrons near the lth EC harmonic to provide efficient interaction with the waves,

$$\omega_{\mathrm{RF}} = l\omega_{\mathrm{ce}}/\gamma + k_{||}v_{||}, \tag{6}$$

where $\gamma = (1 - v_{\perp}^2/c^2 - v_{\|}^2/c^2)^{-1/2}$ is the relativistic factor, $v_{\perp}$ and $v_{||}$ are the components of the velocity perpendicular and parallel to the magnetic field, and $k_{||} = \omega_{\mathrm{RF}}N_{||}/c$ is the component of the wave vector k parallel to B and c is the speed of light. Even for plasmas with moderate electron temperature the Doppler downshift of the resonance is important in the case of EBWs because while approaching the resonance they can develop very large $k_{||}$. EC resonance and its lower harmonics provide very strong absorption of EBWs even at low temperatures. Usually the power carried by EBW is totally damped at the first met EC harmonic.

EBW CD start-up in ST involves the following steps [22]: first, in the presence of the fundamental EC resonance within the vessel provided by a toroidal field, as for conventional ECH start-up, an appropriate level of vertical field is applied with the minimum at the mid-plane of the machine. Carefully timed and of the appropriate magnitude, pulsed gas is injected into the vessel, followed by the launch of the ordinary polarized (O-mode) RF beam from the low-field side of the ST. The RF beam causes breakdown and initial ionization around EC resonance layer. Gas injection programming is the way to ensure that the plasma that forms around the EC resonance it not over-dense. The method also requires the appropriate density conditions during the second phase when the EBW waves are generated. For reasons that are described later, it is necessary to launch the wave either from above or below the mid-plane, as shown in figure 13. It is important that the density of the resulting plasma remains well below the O-mode cut-off, so that the incident RF beam is not refracted by the

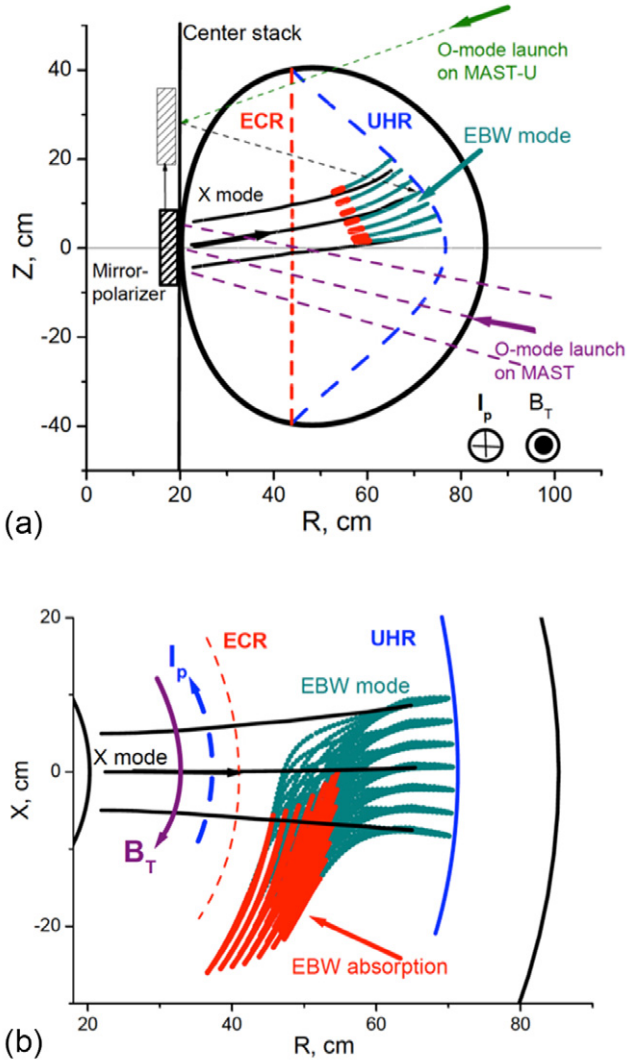

Figure 13. Schematic diagram overlaying ray-tracing simulations of the EBW start-up experiment on MAST and a proposed launch geometry for MAST-U which requires the mirror polarizer to be installed at Z $\sim$ +30 cm. Separation of EC and UH resonances was enhanced for illustration purposes: (*a*) poloidal cross-section showing how the O-mode launched from below the mid-plane mode converts into the X-mode at the mirror polarizer. The X-mode propagates through EC resonance and then mode converts into the EBW mode at UHR. The EBW mode propagates back to the higher field and is rapidly absorbed at the Doppler shifted EC resonance. (*b*) Toroidal cross-section of the same ray-tracing simulations illustrates how fast EBW develops $k_{||}$ while approaching EC resonance, reproduced with permission from [22].

ECH generated plasma. This allows the O-mode to propagate to the high-field side region to the ST center stack.

On MAST, a grooved mirror polarizer is incorporated into the graphite tile covering the center stack at the mid-plane. The incident horizontally polarized wave (O-mode) upon reflection from the mirror polarizer changes polarization to vertical i.e. mode converts into the X-mode wave. The reflected wave can now propagate back towards the low-field side region of the vessel. Absorption of the X-mode at the fundamental EC resonance is anomalously small if the wave propagates perfectly perpendicular to the magnetic field. Hence all

the X-mode polarized RF power can pass through the EC resonance. In large aspect ratio tokamaks, with the port access to the high-field side, the X-mode RF beam can be directly launched from the high-field side, so that the grooved polarizer is not required [76]. The X-mode wave then passes through the EC resonance layer and soon after that encounters the upper hybrid resonance (UHR). While the wave approaches the UHR layer its refractive index rapidly increases resulting in the wave slowing down. Finally the X-mode is mode converted into the EBW mode in the vicinity of UHR.

Being a backward wave by its nature the mode converted EBW propagates back to the high-field side from the UHR layer (figure 13). The wave vector of EBW is essentially perpendicular to the UHR layer because the refractive index perpendicular to the magnetic field $N_\perp$ dominates $N_\parallel$ by about two orders of magnitude.

If the initial O-mode was launched from below the mid-plane the EBW wave absorption will occur predominantly above the mid-plane, as shown in figure 13. Such launch geometry was used on MAST because of accessibility limitations for the RF launcher. On MAST-U it is planned to inject RF power from the location well above the mid-plane to ensure that the X-to-EBW mode conversion occurs above the mid-plane to generate predominantly positive $N_\parallel$ at the origin of EBW mode in the closed flux surface configuration. At the origin, the sign of $N_\parallel$ determines whether EBW interacts with electrons moving along or opposite the magnetic field as follows from equation (6). The sign of $N_\parallel$ is given by the projection of the wave vector k on the local magnetic field near the UHR where EBW originated. In tokamak plasmas usually $B_T \gg B_P$ hence $k_{||} \approx k_T + k_P B_P/|B|$, where k_T and k_P are the toroidal and poloidal components respectively. In the UHR layer EBW has typically $|k_P B_P/|B|| \gg |k_T|$, except for the vicinity of the mid-plane, thus the sign of $k_{||}$ is mainly determined by the sign of $k_P B_P/|B|$. As EBW propagates towards the EC resonance, $k_{||}$ is developed due to poloidal plasma inhomogeneity, resulting in a different sign of $k_{||}$ above and below the mid-plane. Moreover, $k_P B_P/|B|$ changes sign if the plasma current is reversed and remains unchanged if the toroidal field is reversed.

The k vector projection is also influenced by the local plasma density, which can increase or decrease the local UHR curvature compared with the vertical field curvature in the open field line region.

A positive $N_\parallel$ results in interaction with electrons moving opposite to the direction of the plasma current, resulting in co-current drive for the plasma current direction in the MAST tokamak. However, before the flux surfaces closure, the local curvature of vertical field lines is usually smaller than the UHR layer curvature resulting in $k_P B_P/|B| < 0$, since the wave vector k is always perpendicular to the UHR layer. In this configuration EBW would drive counter-current in the same location, as was seen in early MAST experiments.

To correct for this, the radial magnetic field coils on MAST are used to shift the plasma vertically up to provide the right curvature of the flux surfaces to have $N_\parallel > 0$ at the UHR layer during the open field phase. Then after the flux surfaces closure plasma must be shifted down, back to the mid-plane again in order to provide $N_\parallel > 0$ at UHR, thus permitting co-current drive. The successful demonstration of this method is shown in figure 14, in which the radial field is initially energized to displace the plasma above the machine mid-plane to drive positive current during the open field line configuration phase, and the vertical field current reduced to zero, to re-center the plasma so that the favorable condition for CD also exists in the same region after flux closure. Recently using this technique the plasma currents up to 73 kA have been achieved with only 60 kW of 28 GHz RF power injected into the MAST vessel [74].

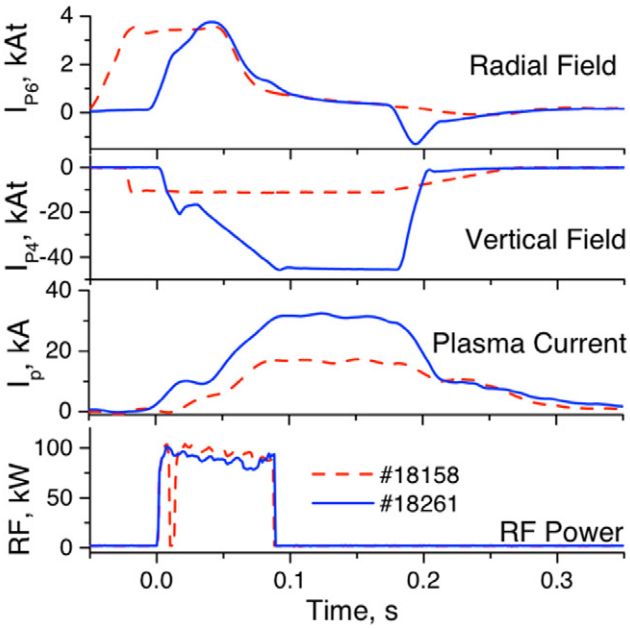

Figure 14. EBW experimental results from MAST. The top trace shows the current in the upper radial field coil while the current in the lower coils is in the opposite direction. These currents shift the plasma center to be above the mid-plane during the open-field line phase. After closed flux surfaces begin to form, the current in these coils is reduced to zero so the plasma is now centered and EBW continues to drive current in the co-direction. The second trace shows the effect of a vertical field ramp. The resulting plasma current is shown on the third trace and the RF pulse on the last, reproduced with permission from [22].

5. Summary

Substantial progress has been made in ST plasma start-up without reliance on the CS. Methods based on transient coaxial helicity injection and local helicity injection have demonstrated start-up at plasma current levels well over 100 kA. These currents have been coupled to conventional inductive drive to demonstrate discharge purity and compatibility with conventional ST operation. These are planned to undergo final tests on the soon to be operational NSTX-U device at PPPL. EBW start-up has generated over 70 kA on MAST and will be an important part of the MAST-U research program. It is also planned to be tested on NSTX-U. Methods based on ECH/EBW start-up are also being studied on the LATE device, and in the much larger and steady-state capable QUEST device, both in Japan. The capability for

LHCD start-up is being developed on the TST-2 device in Tokyo. Methods based on induction from the outer PF coil have generated 100 kA of current on both JT-60U and DIII-D tokamaks. Merging compression and double null merging start-up, first developed on START and MAST have generated over 300 kA of start-up current using PF coils located inside the vacuum vessel. Capability of these methods for current generation with coils located outside the vacuum vessel is now being developed on the UTST device in Japan, in which 50 kA has already been demonstrated. It will also be tested on the VEST [77] device, which is going to be operational soon in South Korea.

Acknowledgments

We would like to thank Dr Irina Voitsekhovitch of CCFE and Dr Dennis Mueller of PPPL for reviewing the document. We would also like to thank Dr Aaron Redd of the Pegasus group at the University of Wisconsin, and Dr Devon Battaglia of PPPL for reviewing the section on Helicity injection start-up. We also thank Professor Wonho Cho of the Korea Advanced Institute of Science and Technology (KAIST) for providing figure 6. This work is supported by US DOE Contracts DE-FG02-99ER54519 and DE-AC02-09CH11466. The work was part-funded by the RCUK Energy Program [under grant EP/I501045]. To obtain further information on the data and models underlying this paper please contact PublicationsManager@ccfe.ac.uk. The views and opinions expressed herein do not necessarily reflect those of the European Commission.

References

[1] Artsimovich L A 1972 Tokamak devices *Nucl. Fusion* **12** 215
[2] Peng Y-K M 2000 The physics of spherical torus plasmas *Phys. Plasmas* **7** 1681
[3] Voss G M *et al* 2008 Conceptual design of a component test facility based on the spherical tokamak *Fusion Eng. Des.* **83** 1648
[4] Menard J E *et al* 2012 Overview of the physics and engineering design of NSTX upgrade *Nucl. Fusion* **52** 083015
[5] Peng Y-K M *et al* 2009 Remote handling and plasma conditions to enable fusion nuclear science R&D using a component testing facility *Fusion Sci. Technol.* **56** 957
[6] Sykes A 1994 Progress on spherical tokamaks *Plasma Phys. Control. Fusion* **36** B93
[7] Raman R *et al* 2003 Demonstration of plasma startup by coaxial helicity injection *Phys. Rev. Lett.* **90** 0750005
[8] Raman R, Mueller D and Nelson B A 2010 Demonstration of tokamak ohmic flux saving by transient coaxial helicity injection in the National Spherical Torus Experiment *Phys. Rev. Lett.* **104** 095003
[9] Eidietis N W, Fonck R J, Garstka G D, Unterberg E A and Winz G R 2007 *J. Fusion Energy* **26** 43
[10] Sykes A *et al* 2001 First results from MAST *Nucl. Fusion* **41** 1423
[11] Cox M *et al* 1999 The Mega Amp Spherical Tokamak *Fusion. Eng. Des.* **46** 397
[12] Ono Y, Kimura T, Kawamori E, Murata Y, Miyazaki S, Ueda Y, Inomoto M, Balandin A L and Katsurai M 2003 First and second-stable spherical tokamaks in reconnection heating experiments *Nucl. Fusion* **43** 789
[13] Yamada T *et al* 2010 Double null merging start-up experiments in the University of Tokyo spherical tokamak *23rd IAEA FEC 2010 Proc. (Daejeon, Republic of Korea, 11–16 October 2010)* paper EXS/P2-19 (www-pub.iaea.org/mtcd/meetings/PDFplus/2010/cn180/cn180_papers/exs_p2-19.pdf)
[14] Leuer J A *et al* 2011 Solenoid-free startup experiments in DIII-D *Nucl. Fusion* **51** 063038
[15] Ushigome M *et al* 2006 Development of completely solenoidless tokamak operation in JT-60U *Nucl. Fusion* **46** 207
[16] Forest C B, Hwang Y S and Ono M 1992 Internally generated currents in a small-aspect ratio tokamak geometry *Phys. Rev. Lett.* **68** 3559
[17] Forest C B *et al* 1994 Investigation of the formation of a fully pressure-driven tokamak *Phys. Plasmas* **1** 1568
[18] Hanada K *et al* 2011 Non-inductive start up of QUEST plasma by RF power *Plasma Sci. Technol.* **13** 308
[19] Yoshinaga T, Uchida M, Tanaka H and Maekawa T 2006 Spontaneous formation of closed-flux torus equilibrium via current jump observed in an electron-cyclotron-heated plasma *Phys. Rev. Lett.* **96** 125005
[20] Ejira A, Takase Y and Oosako T 2009 Non-inductive plasma current start-up by EC and RF power in the TST-2 spherical tokamak *Nucl. Fusion* **49** 065010
[21] Jobes F *et al* 1984 Formation of a 100-kA tokamak discharge in the Princeton Large Torus by lower hybrid waves *Phys. Rev. Lett.* **2** 1005
[22] Shevchenko V F *et al* 2010 Electron Bernstein wave assisted plasma current start-up in MAST *Nucl. Fusion* **50** 022004
[23] Mueller D 2013 The physics of tokamak start-up *Phys. Plasmas* **20** 058101
[24] Gates D A, Jun C, Zatz I and Zolfaghari A 2010 All-metal transformer core for a low aspect ratio tokamak *Fusion Eng. Des.* **86** 41
[25] Bellan P M 2000 *Spheromaks: A Practical Application of Magnetohydrodynamic Dynamos and Plasma Self-Organization* (London: Imperial College Press)
[26] Taylor J B 1986 Relaxation and magnetic reconnection in plasmas *Rev. Mod. Phys.* **58** 741
[27] Woltjer LJ 1958 A theorem on force-free magnetic fields *Proc. Natl Acad. Sci. USA* **44** 489
[28] Jarboe T R 1989 Formation and steady-state sustainment of a tokamak by coaxial helicity injection *Fusion Technol.* **15** 7
[29] Ono M *et al* 1987 Steady-state tokamak discharge via dc helicity injection *Phys. Rev. Lett.* **59** 2165
[30] Raman R *et al* 2001 Non-inductive current generation in NSTX using coaxial helicity injection *Nucl. Fusion* **41** 1081
[31] Raman R, Mueller D and Jardin S C 2013 Non-inductive plasma start-up on NSTX and projections to NSTX-U using transient CHI *Nucl. Fusion* **53** 073017
[32] Redd A J *et al* 2007 Coaxial helicity injection in open-flux low-aspect-ratio toroidal discharges *Phys. Plasmas* **14** 112511
[33] Nelson B A *et al* 2011 Demonstration of 300 kA CHI-startup current, coupling to transformer drive and flux saving on NSTX *Nucl. Fusion* **51** 063008
[34] Redd A J *et al* 2008 Flux amplification in helicity Injected Torus (HIT-II) coaxial helicity injection discharges *Phys. Plasmas* **15** 022506
[35] Nagata M, Kanki T, Fukumoto N and Uyama T 2003 The internal magnetic field structures and current density profiles in the Helicity Injected Spherical Torus plasma driven by coaxial helicity injection *Phys. Plasmas* **10** 2932
[36] Jarboe T R *et al* 2012 Imposed-dynamo current drive *Nucl. Fusion* **52** 083017

[37] Raman R *et al* 2005 Non-inductive solenoid-free plasma start-up using coaxial helicity injection *Nucl. Fusion* **45** L15–19

[38] Raman R *et al* 2011 Transient CHI start-up simulations with the TSC *Nucl. Fusion* **51** 113018

[39] Ebrahimi F *et al* 2013 Magnetic reconnection process in transient coaxial helicity injection *Phys. Plasmas* **20** 090702

[40] Hooper E B *et al* 2013 Resistive magnetohydrodynamic simulations of helicity-injected startup plasmas in National Spherical Torus eXperiment *Phys. Plasmas* **20** 092510

[41] Ebrahimi F *et al* 2014 Physics of forced magnetic reconnection in coaxial helicity injection experiments in National Spherical Torus Experiment *Phys. Plasmas* **21** 056109

[42] Raman R *et al* 2006 Efficient generation of closed magnetic flux surfaces in a large spherical tokamak using coaxial helicity injection *Phys. Rev. Lett.* **97** 175002

[43] Raman R, Mueller D and Jarboe T R 2011 Experimental demonstration of tokamak inductive flux saving by transient coaxial helicity injection on National Spherical Torus Experiment *Phys. Plasmas* **18** 092504

[44] Raman R *et al* 2009 Solenoid-free plasma startup in NSTX using transient CHI *Nucl. Fusion* **49** 065006

[45] Raman R *et al* 2007 Transient coaxial helicity injection for solenoid-free plasma startup in HIT-II *Phys. Plasmas* **11** 022504

[46] Taylor G, Bertelli N and Ellis R A 2013 Physics design of a 28 GHz electron heating system for National Spherical Torus Experiment Upgrade *20th Topical Conf. on RF Power in Plasmas (Sorrento, Italy, 25–28 June 2013)*

[47] Bayliss R A *et al* 2011 Zero-beta modeling of coaxial helicity injection in HIT-II spherical torus *Phys. Plasmas* **18** 094502

[48] Redd A J *et al* 2010 Non-solenoidal startup as a path to high normalized current operations in the Pegasus Toroidal Experiment *Proc. 37th EPS Conf. (Dublin, Ireland, 21–25 June 2010)* paper P4.183

[49] Taylor R J *et al* 1989 H-mode behavior induced by cross-field currents in a tokamak *Phys. Rev. Lett.* **63** 2365

[50] Darrow D S *et al* 1990 Properties of dc helicity injected tokamak plasmas *Phys. Fluids* B **2** 1415

[51] Hwang Y S *et al* 1992 Reconstruction of current density distributions in the CDX-U tokamak *Rev. Sci. Instrum.* **63** 4747

[52] Fiksel G *et al* 1996 High current plasma electron emitter *Plasma Sources Sci. Technol.* **5** 78

[53] Redd A J *et al* 2009 Point-source helicity injection current drive system for the Pegasus Toroidal Experiment *J. Fusion Energy* **28** 203–7

[54] Battaglia D J *et al* 2009 Tokamak startup using point-source dc helicity injection *Phys. Rev. Lett.* **102** 225003

[55] Battaglia D J, Bongard M W and Fonck R J 2011 Tokamak startup using outboard current injection on the Pegasus Toroidal Experiment *Nucl. Fusion* **51** 073029

[56] Redd A J *et al* 2012 Local helicity injection startup and edge stability studies in the Pegasus Toroidal Experiment *Proc. IAEA 24th Conf. (San Diego, USA, 8–13 October 2012)* paper EX/P4-36

[57] O'Bryan J B, Sovinec C R and Bird T M 2012 Simulation of current-filament dynamics and relaxation in the Pegasus Spherical Tokamak *Phys. Plasmas* **19** 080701

[58] O'Bryan J B and Sovinec C R 2014 Simulated flux-rope evolution during non-inductive startup in Pegasus *Plasma Phys. Control. Fusion* **56** 064005

[59] Fonck R J *et al* 2012 Local current injector system for nonsolenoidal startup in a low aspect ratio tokamak *Proc. IAEA 24th Conf. (San Diego, USA, 8–13 October 2012)* paper FTP/P1-19

[60] Kim J, Choe W and Ono M 2004 Time-dependent optimization of initiation phase of the outer PF coil-only inductive start-up of NSTX plasmas *Plasma Phys. Control. Fusion* **46** 1647

[61] Choe W, Kim J and Ono M 2005 Solenoid-free toroidal plasma start-up concepts utilizing only the outer poloidal field coils and a conducting center-post *Nucl. Fusion* **45** 1463

[62] Lloyd B *et al* 1991 Low voltage Ohmic and electron cyclotron heating assisted startup in DIII-D *Nucl. Fusion* **31** 2031

[63] Sykes A *et al* 2008 Start-up in STs *4th IAEA Technical Meeting on Spherical Tori and the 14th Int. Workshop on Spherical Torus (Frascati, Italy, 7–11 October 2008)*

[64] Imazawa R *et al* 2012 First plasma experiment on spherical tokamak device UTST *Elect. Eng. Japan* **178** 20–6

[65] Imazawa R *et al* 2012 Spherical tokamak generation and merging on UTST using ex-vessel poloidal field coils only *Elect. Eng. Japan* **179** 18

[66] Macdonald A D 1966 *Microwave Breakdown in Gases* (New York: Wiley)

[67] Gryaznevich M, Shevchenko V and Sykes A 2006 Plasma formation in START and MAST spherical tokamaks *Nucl. Fusion* **46** S573–83

[68] Uchida M, Yoshinaga T, Tanaka H and Maekawa T 2010 Rapid current ramp-up by cyclotron-driving electrons beyond runaway velocity *Phys. Rev. Lett.* **104** 065001

[69] Maekewa T *et al* 2012 Open field equilibrium current and cross-field passing electrons as an initiator of a closed flux surface in EC-heated toroidal plasmas *Nucl. Fusion* **52** 083008

[70] Hanada K 2013 Recent progress on non-inductive driven plasma start-up and investigation towards EBWCD on QUEST *Int. ST Workshop (York, UK, 16–19 September 2013)*

[71] Takase Y *et al* 2011 Development of a plasma current ramp-up technique for spherical tokamaks by the lower hybrid wave *Nucl. Fusion* **51** 063017

[72] Takase Y *et al* 2013 Non-inductive plasma initiation and plasma current ramp-up on the TST-2 spherical tokamak *Nucl. Fusion* **53** 063006

[73] Peng Y-K M, Fogarty P J and Burgess T W 2005 A component test facility based on the spherical tokamak *Plasma Phys. Control. Fusion* **47** B236

[74] Shevchenko V F *et al* 2014 Long pulse EBW start-up experiments in MAST *Proc. EC-18 Joint ECE and ECRH Workshop (Nara, Japan, 22–25 April 2014)*

[75] Laqua H P 2007 Electron Bernstein wave heating and diagnostic *Plasma Phys. Control. Fusion* **49** R1

[76] Shevchenko V, Baranov Y, O'Brien M and Saveliev A 2002 Generation of non-inductive current by electron-Bernstein waves on the COMPASS-D tokamak *Phys. Rev. Lett.* **89** 265005

[77] Chung K J *et al* 2013 Design features and commissioning of the Versatile Experiment Spherical Torus (VEST) at Seoul National University *Plasma Sci. Technol.* **15** 244